Human-induced changes in South American sediment fluxes from 1984 to 2019

H. O. Fagundes[1,2], A. S. Fleischmann[3], F. M. Fan[1], R. C. D. Paiva[1], D. C. Buarque[4], V. A. Siqueira[1], W. Collischonn[1], P. Borrelli[2,5,6]

[1] Institute of Hydraulic Research, Federal University of Rio Grande do Sul, Porto Alegre, Brazil.
[2] Department of Earth and Environmental Sciences, University of Pavia, Pavia, Italy.
[3] Geospatial Analysis of Amazonian Environment and Territories, Mamirauá Institute for Sustainable Development, Tefé, Brazil
[4] Department of Environmental Engineering, Federal University of Espírito Santo, Vitória, Brazil
[5] Department of Science, Roma Tre University, 00146 Rome, Italy
[6] Department of Biological Environment, Kangwon National University, Chuncheon 24341, Republic of Korea

Corresponding author: Hugo de Oliveira Fagundes, h.o.fagundes@hotmail.com

Key Points:

- Comprehensive analysis of sediment flows changes in SA over the last 36 years
- 51% of the main SA rivers have undergone significant changes
- Amazon deforestation and river damming are the main responsible for changes

Abstract

Sediment flows dynamics (erosion, transport and deposition) have been disrupted in South America (SA), a continent with the highest erosion and sediment transport rates globally. However, the magnitude and spatial distribution of the main drivers of changes have been poorly identified and explored. Here, we performed simulations using a hydrological-hydrodynamic-sediment model to comprehensively estimate the spatial and temporal sediment changes and

trends in SA from 1984 to 2019. We found that 51% of the main SA rivers experienced significant changes in simulated sediment transport (QST) over this period, with 36% due to Amazon deforestation and river damming and 15% due to precipitation changes. We also estimated a 10% reduction in the average sediment delivery to the oceans. Deforestation was responsible for QST changes above 80% in some Amazon sites, and hydropower expansion led to a greater reduction of sediment flows (as high as 80-100%) in the Tocantins, Uruguay, Upper Paraná, lower São Francisco, Desaguadero, and Negro rivers. In addition, our results suggest that reservoirs built in the Amazon region in the last decade are also affecting sediment transport. Our modeling outputs provide unprecedented information about the status of sediment dynamics in SA, and a means to develop evidence-based strategies and transboundary policies related to continental-wide sediment dynamics and the conservation and restoration of ecosystems.

Keywords: Sediment transport, large-scale modeling, reservoir, land use.

1 Introduction

Sediment flows (erosion, transport and deposition) play an essential role providing social, economic, and environmental services. The surface flow, rich in organic and inorganic compounds, supports healthy agriculture and natural fertilization (Montanarella et al., 2016), provides nutrients for aquatic ecosystems (Best, 2019), and helps maintain the structural stability of rivers, shorelines, mangroves, and wetlands (Costanza et al., 1997; Ezcurra et al., 2019; Nagel et al., 2022). However, sediment flows (sand, silt and clay) have been considerably disrupted by accelerating human-induced erosion, sediment trapping in dams, and long-term changes in

49 precipitation patterns (Ezcurra et al., 2019; Grill et al., 2019; Latrubesse et al., 2017; Quinton et
50 al., 2010).

51 Over the last three decades, 60% of South America (SA) territory experienced land use and land
52 cover changes (LULCC), with extensive areas converted into pastures, cropland, and tree
53 plantations, mainly in the Chaco and Amazon ecosystems (Zalles et al., 2021). Over the same
54 period, more than 100 large reservoirs were constructed, with a storage capacity of more than
55 400 billion cubic meters, affecting aquatic species throughout SA. The continent has more than
56 6,800 reservoirs (Mulligan et al., 2020), of which more than 340 are large reservoirs (Lehner et al.,
57 2011). In addition, 1,300 hydroelectric generation reservoirs are under construction or planned in
58 the continent (Zarfl et al., 2015), with 288 only in the Amazon region (Latrubesse et al., 2017).
59 These numbers constantly change due to the new developments and environmental licensing
60 procedures. In addition, several flood and drought events have been recorded in recent years (Cai
61 et al., 2020), with increasing precipitation trends in the Amazon region and decreasing
62 precipitation in Central Argentina and the Brazilian Northeast.

63 These ongoing changes can induce detrimental effects on SA ecosystems (e.g., Central Amazon
64 floodplains and Pantanal), one of the world's richest locations in terms of above-ground, soil, and
65 aquatic biodiversity (Albert et al., 2021; Barbarossa et al., 2020; Kemppinen et al., 2020). For
66 example, unsustainable agricultural expansion requires more fertilizers(Borrelli et al., 2017),
67 which can be responsible for both the water bodies eutrophication and damage to human
68 health(Dissanayake and Chandrajith, 2009). In addition, the reservoirs storage capacity can be
69 considerably reduced by aggradation, threatening the water supply (Wisser et al., 2010). In
70 contrast, lower sediment delivery to the oceans can induce the erosion of coastal terrestrial
71 ecosystems (Ezcurra et al., 2019). Also, floodplains and mangroves are very productive areas

(Costanza et al., 1997) that can be eroded by reducing sediment to the rivers, making them a source of carbon to the atmosphere instead of a sink (Ezcurra et al., 2019). Moreover, a disturbance in sediment flows can also affect the meander migration, generating social and economic damage to riverine communities (Nagel et al., 2022).

Therefore, it is essential to understand the magnitude of changes in sediment fluxes, their associated key drivers, and their role in mitigating ecosystem degradation effects. New insights are needed to narrow the knowledge gap for river sediment dynamics, especially for large geographical domains encompassing transboundary regions like SA river systems. However, the lack of observed data represents a major barrier to develop analyses for large scales (continental or global) that require long time series for many sites (Best, 2019). For these scales, no studies with in situ data have been found in the literature. The most notable work published recently used remote sensing data to show changes in global sediment fluxes (Dethier et al., 2022). However, this work did not show the climatic influence on sediment supply and focused on assessing changes at the mouths of major rivers. This approach does not provide a broad understanding of the sediment processes that occur in the basin. For example, it is known that the concentration of sediments at the mouth of the Amazon River tends to be higher than in upstream regions due to local processes such as resuspension (Fassoni-Andrade and Paiva, 2019). An isolated analysis of this process occurring at the mouth can lead to a misinterpretation of the processes occurring throughout the basin.

In this way, large-scale assessments of sediment fluxes are usually performed using global sediment transport models to characterize their spatial or temporal dynamics. These models were developed to estimate the impact of human activities on sediment delivery to the oceans (Syvitski et al., 2005), characterize rivers in terms of transported sediment loads (Cohen et al., 2013;

Pelletier, 2012), and assess regional trends and variabilities (Cohen et al., 2014). However, they do not typically attempt to understand the relative contributions of precipitation, dams, and LULCC on sediment fluxes. From the literature, we noted that most studies focused on describing changes in sediment fluxes by considering one or two of these drivers (Almagro et al., 2017; Diodato et al., 2020; Forsberg et al., 2017; Huang et al., 2020; Latrubesse et al., 2017; Syvitski et al., 2009; Vörösmarty et al., 2003; Wei et al., 2019), and few have provided detailed analyses on these changes (Huang et al., 2020; Wei et al., 2019). Some studies have performed integrated analyses with all the aforementioned drivers, but the information was presented for specific locations or with a broad perspective (Li et al., 2020; Macklin and Lewin, 2019).

This study provides the first comprehensive analysis of the spatiotemporal changes in sediment fluxes in SA over the last 36 years (1984 to 2019), accounting for changes in precipitation, dams, and land use and land cover (LULC). To pursue this goal, we simulated multiple scenarios with the continental-scale sediment model MGB-SED AS (acronym in Portuguese for 'Modelo de Grandes Bacias', Fagundes et al., 2021) using daily precipitation, eight LULC maps, and 234 large dams. In addition, relationships between these changes and impacts on ecosystems are presented. These simulations enabled us to isolate each driver's contribution and also to assess their combined effects on sediment flows.

2 Study area

South America (SA, Figure 1-A) is one of the continents with the highest erosion and sediment transport rates globally (Borrelli et al., 2017; Doetterl et al., 2012; Latrubesse et al., 2005), has a large biodiversity (Kemppinen et al., 2020), is one of the few regions having free-flowing rivers

(Grill et al., 2019), and contributes significantly to global food production (Sartori et al., 2019). Most of SA is located in tropical regions that have little interannual variability between sunrise and sunset and receive high solar incidence. The Intertropical Convergence Zone (ITCZ) directly influences the establishment of dry and rainy seasons; El Niño events; and the South Atlantic Convergence Zone (SACZ), which causes heavy precipitations in the summer. Annual precipitation variability is strong, with desert regions in Chile (0.05 to 10 mm/year, Bozkurt et al., n.d.) and very humid regions in Colombia (~10,000 mm/year, Latrubesse et al., 2005). The Amazon, Orinoco, Paraná and Magdalena rivers are the main sediment transporters, meaning 44%, 14%, 11% and 3%, respectively, of total South America sediment discharges values to the ocean (Fagundes et al., 2021). In addition, floodplains in SA has an important role in retaining 12% of total suspended sediment carried by the rivers (Fagundes et al., 2021).

However, the rapid expansion of agriculture on the continent (Figure 1-B) in recent decades (Song et al., 2018; Zalles et al., 2021) is accompanied by increasing erosion rates, directly affecting food production and the economy (Borrelli et al., 2017; Sartori et al., 2019). In addition, many existing reservoirs (Figure 1-C) have been reducing the sediment load in rivers and oceans (Syvitski et al., 2005), causing negative impacts in these regions (Syvitski et al., 2009). Nevertheless, the concern is even greater with SA planned reservoirs (see Figure S1 - Supporting Information S1), especially in the Amazon region, as they may dramatically affect river connectivity (Grill et al., 2019), sediment exchange between rivers and floodplains (Latrubesse et al., 2017), biodiversity (Albert et al., 2021; Barbarossa et al., 2020), fish migration (Forsberg et al., 2017), and deltas (Dunn et al., 2019). SA has also been showing changes in annual precipitation (Figure 1-D), with increasing trends in intense rainfalls in some regions (e.g. Amazon, Diodato et al., 2020), while others have experienced severe droughts in recent years (e.g. Northeast Brazil, Marengo et al., 2022).

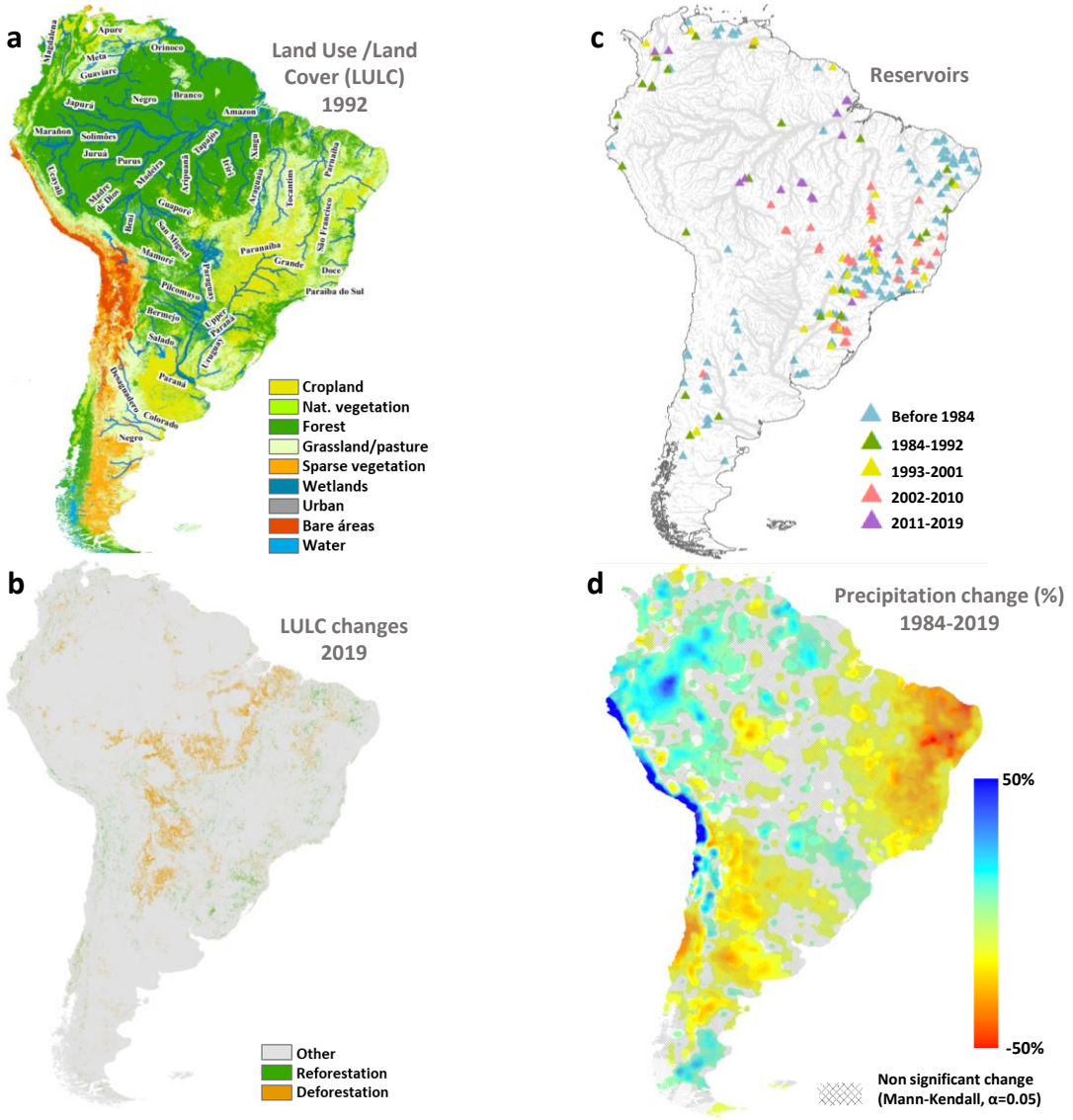

Figure 1. Overview of South America changes. a, main changes in land use/ land cover between 1992 and **b**, 2019, using LULC data from European Space Agency (http://www.esa-landcover-cci.org/). **c**, 234 large dams (storage capacity > $10^6 m^3$) from Yigzaw dataset (see methods section), *Brazilian Water National Agency* and Brazilian *National Electric System Operator*. **d,** trends of precipitation changes from 1984 to 2019 using daily precipitation from the Multi-Source Weighted Ensemble Precipitation – MSWEP v1.1 dataset until 2014, and from 2015 onward using the NASA Global Precipitation Measurement Mission – GPM dataset.

3 Methods

3.1 Modeling South American hydrology and sediments: the MGB-SED AS model

The MGB-SED model results from the coupling of a sediment module (Buarque, 2015) with the MGB hydrological model (Collischonn et al., 2007; R. C. D. Paiva et al., 2011; Pontes et al., 2017).

This model has shown ability to simulate sediment erosion, transport and deposition at large scales (Fagundes et al., 2019, 2021, 2020; Föeger et al., 2022), and the hydrological module has been applied in many tropical watersheds to address different questions (Fleischmann et al., 2019a, 2018; R. C. D. Paiva et al., 2011; Pontes et al., 2017; Siqueira et al., 2018).

The MGB-SED AS model (Fagundes et al., 2021) was developed to investigate the spatial and temporal dynamics of suspended sediment flows in South America. This model resulted from the coupling between the sediment module and the hydrologic-hydrodynamic model MGB-SA, presented by Siqueira et al. (2018). According to Fagundes et al. (2021), this configuration was mainly chosen due: (i) MGB-SA is the first fully coupled hydrologic-hydrodynamic model, developed for regional scales, applied for SA's continental domain; and (ii) the model has a high temporal resolution (daily outputs) and was validated in most of SA using in situ and other sources of hydrological data, showing that hydrological variables were well represented (graphical and statistical analysis). Both MGB-SA (Siqueira et al., 2018) and MGB-SED AS (Fagundes et al., 2021) showed better performance to global models in simulate hydrological and sediment variables. The MGB-SED AS model (Fagundes et al., 2021) simulates suspended sediment flows for the medium to large South American (SA) rivers (river reaches with drainage areas larger than 1,000 km²). The model has a sediment module(Buarque, 2015) coupled to the MGB–SA hydrologic-hydrodynamic model (Siqueira et al., 2018). The main model's forcing variable is the daily precipitation and it was calibrated and validated in most continental areas using in situ data for both hydrological and sediment variables. The model is described in the following sections.

3.1.1 Hydrological-hydrodynamic module

The MGB-SA is a continental-scale hydrologic-hydrodynamic model developed for the South American domain (Siqueira et al., 2018). It uses simplified mathematical relations to describe

runoff generation processes and physically based equations to compute evapotranspiration and channel routing processes. The main hydrological processes simulated by the model are (i) canopy interception; (ii) soil infiltration; (iii) evapotranspiration; (iv) routing of surface, subsurface, and groundwater runoff (hillslope routing); and (v) hydrodynamic propagation in river networks.

The model is discretized using a semi-distributed approach, where basins are divided into unit-catchments according to the underlying topography and a pre-defined river length, and further into Hydrological Response Units (HRUs) based on combinations of soil type and land cover. Vertical water balance and evapotranspiration (calculated with Penman-Monteith equation) are computed at the HRU level, and river routing is computed at the unit-catchment scale.

(Pontes et al., 2017)(Collischonn et al., 2007)(Kouwen et al., 1993)MGB–SA uses the local inertial equation (Bates et al., 2010) to route streamflow along the drainage network and to compute stored volume, flooded area, discharge, and river water levels. The water surface elevation is assumed homogeneous along a given unit-catchment. Recent works have assessed the impact of spatial discretization on MGB simulated variables and have shown that the effect on river discharges tends to be small compared with those on water level and flood extent (Fan et al., 2021a; Fleischmann et al., 2019b). Floodplains are represented as storage areas in which water can be lost through evaporation. Infiltration of floodplain water into the unsaturated soils is also computed. When compared with the full 1D Saint-Venant equations, the local inertial method is relatively simple as it has an explicit solution, and has been successfully applied to represent low-slope rivers and floodplain effects in flood inundation/river routing models with scales ranging from regional (Fleischmann et al., 2018; Getirana et al., 2017) to global (Yamazaki et al., 2013). On the other hand, it requires a smaller time step (typically 3-4 minutes) to avoid numerical instability, and has limitations to simulate river regimes with relatively high flow velocity as the

198 advective inertia term – which is neglected in the local inertial model – may become important
199 (Bates et al., 2010; Pontes et al., 2017, Fleischmann et al., 2018)

200 ***3.1.2 Sediment module***

201 The sediment module is divided into basin, river, and floodplain modules. The basin module
202 computes rill and interrill erosion of hillsides using the Modified Universal Soil Loss Equation
203 (MUSLE – Equation 1)(Williams, 1975).

204 $$Sed = \alpha.(Q_{sur} * q_{peak} * A)^{\beta}.K.C.P.LS_{2D} \quad (1)$$

205 where Sed [t/day] is the sediment yield, Q_{sur} [mm/day] is the specific runoff volume, q_{peak} [m³/s]
206 is the peak runoff rate, A [ha] is the unit-catchment area, K [0.013 · t · m² · h/m³ · t · cm] is the
207 soil erodibility factor, C [dimensionless] is the cover and management practices factor,
208 P[dimensionless] is the conservation practices factor, LS_{2D} [dimensionless] is a bidimensional
209 topographic factor, and α and β are the equation fit coefficients, with values originally estimated
210 at 11.8 and 0.56 (Williams, 1975), respectively. We used the same parameter values set for the
211 first application of the MGB-SED AS model (Fagundes et al., 2021).

212 The sediment volume estimated by MUSLE is divided into three particle classes (sand, silt, and
213 clay) and is discharged into the river through three linear reservoirs, that store these sedimentsIn
214 the river drainage network, each of three sediment loads is routed from upstream to downstream.
215 Fine loads (silt and clay) are routed using the 1D advection transport equation without the
216 diffusion term, and the sediments are transported in suspension without deposition in the
217 channel. Sands, considered bedload, are routed using the Exner sediment continuity equation and
218 the Meyer-Peter and Müller transport capacity equation to quantify the channel's transport,
219 erosion, or deposition (Buarque, 2015).

The characteristic diameters adopted for silt and clay particles were 0.016 mm and 0.001 mm, respectively. These assumed values have led to satisfactory results in a previous study (Fagundes et al., 2021). We began our simulations using a characteristic sand diameter value of 0.1 mm. However, because bedload has strongly heterogeneous characteristic diameters, especially when rivers with high and low slopes are compared, we developed an empirical equation to estimate the characteristic sand diameter. After an exhaustive search for South American bedload data in several journals and repositories (in Portuguese, Spanish, and English), we selected the D50 diameter from 14 river reaches (Carvalho, 2009; Fantin-Cruz et al., 2020; Filho, 2016; Latosinski et al., 2017; J. B. D. de Paiva et al., 2011; Paiva, 1988, 2007; Rizzardi, 2013; Strasser, 2008; Wiegand, 2009). We performed a unique regression (R^2=0.21) using D50 diameter against the slope ($Sl, m/km$) (estimated from a Digital Elevation Model - DEM), yielding Equation 2:

$$Dsand = 0.4476 Sl^{0.0776} \quad (2)$$

where $Dsand$ (m) is the characteristic diameter of sand for a specific river reach.

In the floodplain module, suspended sediment exchanges between rivers and floodplains are computed assuming that floodplains have a zero longitudinal velocity and complete mixing. These assumptions imply that concentrations of silt and clay are uniform in the vertical profile. Sediment deposition is computed using the fall velocity equation (Equation 3)(Wu and Wang, 2006). Sediments that are not deposited flow back to the main channel.

$$\omega_j = \frac{Mv}{Nd}\left[\sqrt{\frac{1}{4} + \left(\frac{4N}{3M^2} {D_{*_j}}^3\right)^{\frac{1}{np}}} - \frac{1}{2}\right]^{np} \quad (3)$$

where

$$M = 53.5e^{-0.65Sp} \quad (4)$$

$$N = 5.65e^{-2.5Sp} \quad (5)$$

$$np = 0.7 + 0.9Sp \quad (6)$$

$$D_{*,j} = d\left[\frac{\left(\frac{\rho_s}{\rho} - 1\right)g}{v^2}\right]^{\frac{1}{3}} \quad (7)$$

and where v is water kinematic viscosity (10^{-6} m²/s); Sp is the Corey shape factor, taken as 0.7 (WU, 2008); d[m] is the representative nominal diameter of the particle class; $D_{*,j}$ is the non-dimensional diameter for the j particle size; ρ_s/ρ is the sediment-specific gravity; and g is the gravity acceleration (9.8 m/s²).

3.1.3 Reservoir module

Within the MGB-SED AS model framework, the representation of reservoirs involves the regulation of water inflows at a given dam location and sediment trapping along the reservoir lake. These two aspects are detailed in the following two sections.

3.1.3.1 Water regulation by dams

The regulation effect of a given dam is simulated using an offline routine, i.e., the hydrodynamics of a given unit-catchment associated with a dam are replaced by a level-pool routine (lumped reservoir). Thus, the dam inflow is estimated as the inflow to that unit-catchment, using a uniform flow as the boundary condition for upstream unit-catchments with an average water slope

259 estimated from the DEM. The dam level-storage relationship is obtained from national and global
260 reservoir databases. Direct lake evaporation was also included and computed using the Penman
261 equation (Shuttleworth, 1993).

262 The dam outflow is simulated with a simple operation scheme (Hanasaki et al., 2006; Shin et al.,
263 2019).The suitability of this scheme for estimating large-scale reservoir regulation was recently
264 shown (Fleischmann et al., 2021) for a test case of more than 30 reservoirs in the Paraná River
265 Basin in Brazil. They concluded that although the proposed approach (Shin et al., 2019) is generic
266 and simple, it provides reasonable estimates and is useful in evaluating regional hydrologic regime
267 scale alterations.

268 The adopted scheme is a daily inflow-and-demand-based rule suitable for hydropower dams,
269 which do not withdraw water from the system. This approach is reasonable for South America,
270 where most dams are used for hydropower generation. Equation 8 defines the dam outflow:

271 $$Q(i,t) = R_i K_{i,y} I_m + (1 - R_i) I_t \quad (8)$$

272 where $Q(i,t)$ is the ith dam outflow at daily time step t, R_i is a regulation capacity constant that
273 can be calibrated with observations or estimated with Equation 9 (Shin et al., 2019), and is
274 assumed to be equal zero for run-of-the-river dams ($R_i < 0.1$). I_m and I_t are the annual average
275 and daily dam inflows, respectively, and $K_{i,y}$ is the storage fraction at the beginning of the
276 hydrological year (Equation 10). The hydrological year of each dam is defined as the month where
277 the naturalized (pristine) flow falls below the average (i.e., the beginning of drawdown season)
278 (Hanasaki et al., 2006).

279 $$R_i = \min(1, \alpha c_i) \quad (9)$$

280 $$K_{i,y} = S_{first,y} / \alpha C_i \quad (10)$$

The term c_i is the ratio of the maximum dam storage C_i to the annual average dam inflow ($c_i = C_i/I_m$), $S_{first,y}$ is the storage at the beginning of the hydrological year y, $\alpha_{res}C_i$ is the target storage, and α_{res} is a constant set to 0.85 (Hanasaki et al., 2006). I_m was calculated based on a prior long-term MGB simulation (1984–2019), including dynamic land cover and climate, but not reservoirs. This approximation is reasonable because reservoir regulation has a minor impact on the long-term average discharge (mainly through evaporation).

After estimating $Q(i,t)$, the reservoir storage is updated using equation 11, which represents a lumped (concentrated) reservoir:

$$V_{act}(i,t) = V_{act}(i,t-1) + (I_t - Q(i,t)) * 86400) \quad (11)$$

where $V_{act}(i,t)$ is the ith dam volume at daily time step t.

On the first simulation day for a given reservoir (i.e., the first day of either the MGB simulation or the dam inauguration year), it was assumed to be full. The dams were inserted into the model in their respective inauguration years to account for the interannual changes in dam storage across the continent.

As described next,, a set of equations (12-15) were adopted to ensure the stability of the numerical scheme and to prevent unphysical behavior (e.g., to avoid negative storage).

For the run-of-the-river reservoirs:

- If the reservoir storage is under 90% after computing $Q(i,t)$ and $V_{act}(i,t)$, we compute a new discharge (Equation 12) and volume (Equation 11).

$$Q^1(i,t) = Q(i,t) - \frac{V_{max} - V_{act}(i,t-1)}{86400} \frac{V_{act}(i,t-1)}{V_{max}} \quad (12)$$

where $Q^1(i,t)$ is the updated discharge for daily time step t.

- If this scheme results in a negative volume, we return to the original values estimated using Equation 11 and compute a new outflow discharge using Equation 13.

$$Q^1(i,t) = 0.01\,\frac{V_{act}(i,t-1)}{86400} \tag{13}$$

- If Equation 12 instead results in a negative discharge, we re-compute the updated discharge as:

$$Q^1(i,t) = Q(i,t) - 0.01\,\frac{V_{act}(i,t-1)}{86400} \tag{14}$$

For the reservoirs that are not run-of-the-river reservoirs:

- If the reservoir storage is above 98% (almost overtopping) after computing $Q(i,t)$ and updating the reservoir storage (V_{act}):

$$Q^1(i,t) = Q(i,t) + \frac{V_{act} - 0.98\,V_{max}}{(1-0.98)V_{max}}\,(\max(0.0, I_t - Q(i,t)) \tag{15}$$

- If the reservoir storage is under 20% after computing $Q(i,t)$ and $V_{act}(i,t)$, we follow the process described above for run-of-the-river reservoirs when they are less than 90% full.

3.1.3.2 Sediment deposition in reservoir

To represent the deposition of fine sediments (silt and clay) in reservoirs, we used Equation 16(Julien, 2010),

$$C(i,t,j) = Co(i,t,j)e^{\frac{-X_i\omega_j}{h_i u_i}} \tag{16}$$

where $C(i,t,j)$ is the ith dam downstream sediment concentration at daily time step t for the j particle size (silt or clay); $Co(i,t,j)$ is the ith dam upstream sediment concentration at daily

time step t for the j particle size; X_i is the ith dam longitudinal length; ω_j is the settling velocity (Equation 3) for the jth particle size; h_i is the ith dam average depth (Equation 17); u_i is the ith dam longitudinal velocity (Equation 18).

$$h_i = \frac{V_{act}}{Ares_i} \quad (17)$$

where $Ares_i$ is the ith dam surface area.

$$u_i = \frac{I_t}{h_i \left(\frac{Ares_i}{X_i}\right)} \quad (18)$$

For coarse sediments (sands), we assumed that the total load arriving in the reservoir is deposited.

3.2 MGB-SED AS input data and parameterization

The MGB–SA simulations used the 15 arcsec HydroSHEDS flow direction map (Lehner et al., 2008) and a 1,000km² minimum drainage area threshold. The unit-catchment discretization used a fixed river length of 15km. Floodplain topography was estimated at the sub- unit-catchment level using the Height Above Nearest Drainage (HAND) computed from the Bare-Earth SRTM v.1 DEM (O'Loughlin et al., 2016). The river hydraulic geometry (bankful width and depth) was specified using a global dataset (Andreadis et al., 2013) with additional information from regional studies (Beighley and Gummadi, 2011; Paiva et al., 2013; Paiva et al., 2011; Pontes, 2016). Manning's roughness coefficient was set to 0.03 for the entire continent, as is typical in large-scale hydrodynamic modeling (Siqueira et al., 2018).

The simulation from 1984 to 2019 was performed using daily precipitation from the Multi-Source Weighted Ensemble Precipitation – MSWEP v1.1 dataset (Beck et al., 2017) until 2014 and using the NASA Global Precipitation Measurement Mission – GPM dataset (Skofronick-Jackson et al.,

2017) from 2015 onward. For the GPM data, a correction of the precipitation bias was performed so that the values were more compatible with the MSWEP data. This correction was performed using the quantile-quantile method, parameterized by the gamma function. Long-term averages (climate normals) for surface air temperature, atmospheric pressure, incoming shortwave solar radiation, relative humidity, and wind speed were obtained from the Climate Research Unit (CRU) Global Climate v.2 data (New et al., 2002)and were used to compute evapotranspiration.

While a previous application using the MGB-SED AS (Fagundes et al., 2021) used the South America HRU's map (Fan et al., 2015) to simulate the influence of land use and land cover (LULC) changes, we used eight LULC maps from European Space Agency (http://www.esa-landcover-cci.org/) and built the HRU's maps for the following years (simulated period): 1992 (1984-1992), 1995 (1993-1995), 1998 (1996-1998), 2001 (1999-2001), 2005 (2002-2005), 2010 (2006-2010), 2015 (2011-2015) and 2019 (2016-2019). We used a short interval in the early years because according to literature (Zalles et al., 2021) LULC changes in this period were higher than those observed in the recent years. The maps have spatial resolution of 300m. We used the same base of the South America HRU's map (Fan et al., 2015) to represent soil type (shallow and deep).

The input data to compute the MUSLE equation in the sediment module is the same as used in the previous application of the MGB-SED AS. The K factor is computed based on the percentages of silt, clay, sand, and organic carbon comprising the soil from the Food and Agriculture Organization (FAO) of the United Nations (FAO/UNESCO, 1974); LS_{2D} is based on the Bare-Earth SRTM v.1 DEM (O'Loughlin et al., 2016); P is assumed to be 1; and C is computed as in previous studies (Benavidez et al., 2018; Buarque, 2015; Fagundes et al., 2021). For each HRU map, the C values changed according to soil cover.

The major difference between the MGB-SED AS version used here and the previous version (Fagundes et al., 2021) is the inclusion of sediment trapping by reservoirs at the continental level. Here, we used 234 large dams (storage capacity > $10^6 m^3$) from the Yigzae dataset(Yigzaw et al., 2018), *Agência Nacional de Águas do Brasil* (ANA) and *Operador Nacional do Sistema Elétrico do Brasil* (ONS). ANA and ONS are Brazilian state agencies. The reservoirs were selected using the following three criteria: (i) they are currently operational; (ii) there are available level-area-volume relationships; (iii) they are not located in headwater unit-catchments (i.e., a drainage area of ~1.000 km^2). Using area and volume information, we fitted a fourth-degree polynomial for each reservoir, which was used to compute the daily surface area from the daily stored volume. When the longitudinal dam lengths were unavailable, they were estimated using visual analysis and geographic information system tools from satellite images.

3.3 Validation of the reservoir and sediment modules

Reservoirs were validated comparing water discharge from 376 in-situ stations against simulated data with and without reservoirs. Using observed and simulated data we computed the Skill Score (SC, Equation 19, Figure S2 - Supporting Information S1) for the Nash-Sutcliffe coefficient (NSE, Nash and Sutcliffe, 1970).

$$SC = \frac{NSE_{reservoir} - NSE}{1 - NSE} \tag{19}$$

The validation of river discharge for 12 gauges located on major regulated river reaches across the continent is presented in Figure S3 - Supporting Information S1. The validation of the simulated reservoirs' volumes and dam outflows using the MGB-SED AS model is shown in Figure S4 - Supporting Information S1. The results demonstrate reasonable model performance,

383 especially in simulating dam volumes dynamics, which is an important variable affecting sediment
384 trapping in the MGB-SED AS model (Equations 16, 17 and 18).

385 After including the reservoirs and obtaining satisfactory results from the model when
386 incorporating LULC changes, we carried out a few manual adjustments to α and β MUSLE
387 parameters values through trial and error. The model performance for sediment flows was
388 evaluated in three different stages: (i) we computed percent BIAS (%) of simulated suspended
389 sediment discharge (QSS, silt+clay) relative to observed QSS, considering the period of 1992–2009
390 and the same 595 sediment stations used in the previous MGB-SED AS simulation (Fagundes et
391 al., 2021). Observed data were obtained from *Agência Nacional de Águas do Brasil*, *Base de Datos*
392 *Hidrológica Integrada da Argentina* (BDHI) and I*nstituto de Hidrologia, Meteorologia e Estudos*
393 *Ambientais da Colômbia* (IDEAM) used in the previous MGB-SED AS simulation (Fagundes et al.,
394 2021) (Figure S5 - Supporting Information S1); (ii) we compared the annual and daily simulated
395 and observed sediment bedload (Figure S6 - Supporting Information S1). Bedload data were
396 collected from local and regional studies (Alarcón et al., 2003; CNEN/CDTN - Centro de
397 Desenvolvimento da Tecnologia Nuclear and IFNMG/Campus Januária - Instituto Federal do Norte
398 de Minas Gerais, 2020; Gamaro et al., 2014, 2011; Latrubesse et al., 2009; Martins et al., 2009;
399 Martins and Stevaux, 2005; SZUPIANY et al., 2005) using other approaches (e.g., acoustic
400 techniques to monitor fluvial ripples). It should be mentioned that both daily and annual bedload
401 data are extremely scarce for large South American rivers.

402 In the Figure S7 - Supporting Information S1, we present an example of the reservoir effect in
403 simulated suspended sediment concentration downstream large dams, comparing two
404 simulations considering the presence and absence of reservoirs against observed data from ANA.

3.4 Long-term analysis of sediment changes

We performed three main analyses to understand how sediment fluxes have changed since 1984. Our simulations assumed that precipitation changes daily, reservoirs begin operating from their first operating year (if this occurred before 1984, its operation begins at the start of the simulation), and LULCC. We started the simulations in 1979 and used five years to warm up the model. Three main scenarios were then simulated to isolate the effect of each driver (precipitation, LULC, and reservoirs), and a final simulation was run to understand the synergistic effects of these drivers on sediment flows:

- *Precipitation changes scenario* – LULC map of 1992, reservoir module disabled, and daily precipitation from 1984 to 2019.
- *Reservoir changes scenario* – LULC map of 1992, reservoir module enabled, and 2012 daily precipitation. A daily precipitation series of 36 years was created by repeating the 2012 data. We tested several years, and 2012 was chosen because it represents the median precipitation during the whole simulation period for the entire South American continent.
- *LULC changes scenario* – all LULC maps, reservoir module disabled, and 2012 daily precipitation.
- *Combined effects scenario* - all LULC maps, reservoir module enabled, and daily precipitation from 1984 to 2019.

The first analysis focused on temporal changes. The entire simulated period (36 years) was divided into four nine-year periods (1984–1992, 1993–2001, 2002–2010, 2011–2019). We then computed the annual total sediment discharge (QST) for each scenario and averaged it over each period. We designated 1984–1992 as the baseline period and computed the relative change for the others (Equation 20).

$$Changes\ (\%) = 100x\frac{QST_{tf} - QST_{1984-1992}}{QST_{1984-1992}} \quad (20)$$

where tf is the future period (1993–2001, 2002–2010 or 2011–2019).

The second analysis focused on the global changes using only the combined effects scenario to identify rivers with significant changes. Here we used two statistical criteria to define significant changes: 1) the QST long-term change in a given river was above 5%; 2) the change was statistically significant to the 5% level using the Mann-Kendall test (M-K test, Kendall and Gibbons, 1975). The QST long-term change was computed using linear regression (time vs. QST) for the entire simulated period by comparing the first and last points of the fitted line. We used this approach instead of Equation 20 because we observed that the QST series exhibited great variability due to interannual precipitation variability, which could be misinterpreted if only 9-years averages were considered. For example, the last period (2011–2019) was quite dry over much of eastern South America, and this phenomena could be erroneously interpreted as a trend. In addition to the criteria presented, rivers were considered significantly affected when they presented significant QST changes in more than 40% of the main river length.

The third and final analysis was carried out to identify the main driver responsible for change for each river with a significant change. We observed that changes in the QST series were more abrupt when only reservoirs or LULC changes were considered, especially because they are timely progressive. However, precipitation changes were more variable, with alternations of dry and wet periods. Therefore, to compute long-term changes (%) appropriately for each driver, we used Equation 20 for the Reservoir changes and LULC changes scenarios and the linear adjustment for the Precipitation changes scenario.

Although we computed changes in sediment fluxes for many rivers in South America, we focused our analyses on the major rivers. The major rivers were classified as those with drainage areas greater than 100,000 km² and simulated QST without reservoirs greater than 1,000,000 t/year. The latter criterion was adopted because it considers more natural river conditions. More than one driver could be dominant for specific river reaches in some large rivers. In such cases, the dominant driver was selected based on two criteria: i) if the river was partially affected by both precipitation and LULC, the driver with more range in the river's downstream portion was selected; ii) the reservoir driver was selected when its effect was observed in a stretch with a drainage area greater than 50% of the basin's drainage area.

4 Results and discussions

4.1 Model validation and caveats

Our modeling outputs agree with previous regional studies. For instance, our analyses suggested that sediment flows are increasing in the Upper Tapajós due to deforestation and the consequent increase of erosion (Oestreicher et al., 2017), and increasing in other several regions of Amazon due to precipitation increase (Diodato et al., 2020). At the same time, we estimated a reduction in sediment flows in the Bermejo River due to the precipitation decrease in its upper basin (González and Murgida, 2012), and most recently, in the Lower Madeira and Lower Tapajós rivers due to reservoir building (Grill et al., 2019; Latrubesse et al., 2017).

Our model was satisfactorily validated in simulating reservoir dynamics. By using 376 gauge stations located downstream of dams, streamflow estimates were improved by 40% when compared to simulations without reservoirs (Figure S2 - Supporting Information S1). We also

compared our daily simulated QSS against data from 595 in situ sediment stations (Figure S5 and Figure S7 - Supporting Information S1). In 60% of the stations, the relative error $BIAS$ was between -50% and 100%. We noted an improvement in QSS estimates after including the reservoirs, especially for the São Francisco (Figure S7 - Supporting Information S1), Paraná, and Tocantins rivers, compared to a previous study using the same model (Fagundes et al., 2021). We also compared simulated daily and annual bedload (sand) values against regional estimates, with $BIAS$ values of 582% and 233%, respectively (Figure S6 - Supporting Information S1). These last differences are reasonable for analyses using annual data such as those conducted in this study.

Sediment studies require considerable data, often acquired via traditional approaches using in situ measurements. However, even in this era of big data and big science, there remains a lack of hydrological and sediment data on the world's large rivers (Best, 2019). This picture is even worse when the subject is bedload data. For example, after extensive research in literature, databases, and private institutions, we achieved bedload data only for 11 sites (Figure S6 - Supporting Information S1) in the whole South America domain. This lack of data points to the great challenge in making measurements (that provide reliable results) of bed load in large rivers and the insufficient investment in this field of science.

Therefore, sediment modeling becomes an alternative to support spatial and temporal analysis but still requires good input data and validation processes (Fagundes et al., 2021). In this study, our main limitation was the lack of observed data to calibrate some model components. Furthermore, although Bolivia and Venezuela are regions with high sediment yield, we could not obtain data from these countries. Other limitations include the insufficient representation of lateral erosion, that can be important for meandering rivers (Nagel et al., 2022), as well as gully erosion and landslides that are relevant sediment processes especially for Andean rivers, like

494 Bermejo and Pilcomayo, and can induce underestimates in these regions (Borrelli et al., 2017). In
495 addition, due to our continental domain of analysis, some simplifications were necessary and can
496 be a source of uncertainties. These include equations that represent processes but are not laws
497 of nature, the use of only three sediment sizes (sand, silt and clay), the use of only one capacity
498 transport equation for bedload estimates in all rivers, a simplified dam operation scheme in the
499 hydrological component, the adoption of a single value for the Manning coefficient, and the non-
500 inclusion of sediment sources from mining activities, which can be relevant in some places.

501 Despite the limitations of the model and the associated uncertainties in sediment flux estimates,
502 it is important to note that even in situ observations can have very high uncertainties (>50%,
503 Navratil et al., 2011). More than this, for large scales (continental or global), no studies with in
504 situ sediment data have been found in the literature, and only the recent study of Dethier (et al.,
505 2022) has presented global results using remote sensing data. Thus, sediment transport models
506 have proven to be the best alternative to large-scale assessments of sediment fluxes on large
507 scales (Cohen et al., 2014, 2013; Fagundes et al., 2021; Pelletier, 2012; Syvitski et al., 2005). These
508 models also have the advantage of providing information that makes detailed spatial and
509 temporal analyses of what is happening in the landscape possible, and also intercomparisons
510 between different geographic and climatic regions. More details about the model performance
511 are discussed in the Supporting Information S1 - Text S1.

512 **4.2 Continental analysis in time and space**

513 The MGB-SED AS model has performed well in simulating sediment fluxes previously (Fagundes
514 et al., 2021), and in this study further improvements have been achieved (section 4.1).
515 Nevertheless, the presented results have uncertainties, which are not simple to quantify.

Therefore, the results presented here, especially those that present absolute values, should be regarded with caution.

Our analysis indicates that 51% of the main SA rivers have shown statistically significant changes in simulated sediment transport over the last 36 years (1984–2019). In 36% of the large rivers evaluated (Table 1), changes were directly caused by human activities such as deforestation and river damming, while precipitation alteration has driven changes in 15% of them. Absolute changes in annual sediment transport above 10% were observed in 14 of the 39 main SA rivers. Sediment flow increases were more frequent in the Amazon Basin rivers. By contrast, decreases were detected in the northeast and southeast portions of the continent (e.g., Paraná, Uruguay, Tocantins, and São Francisco rivers).

The average simulated sediment supply from SA rivers to the oceans was 834 million tons per year (Mt/year), decreasing over the analyzed period (Figure 2). From 2011 to 2019, SA delivered 771 Mt/year to the oceans, almost 10 % less than the 849 Mt/year delivered from 1984 to 1992 (Figure 3), which is a different result from a recent study (Dethier et al., 2022). Dethier et al. (2022) observed sediment changes at the mouths of major rivers and concluded that in South America fluxes are increasing. These different findings result from the different approaches used in each study. For example, it is known that the concentration of sediments at the mouth of the Amazon River tends to be higher than in upstream regions due to local processes on the estuary and coast (e.g. resuspension, Fassoni-Andrade and Paiva, 2019), and not due to the increased sediment load coming from the upstream region.

Table 1. Long-term estimates of sediment transport, mean alterations, and dominant drivers of changes for the main South American rivers. A is the drainage area, Q is the water discharge, QSS and QST are the suspended and total sediment discharge, respectively.

River	A (km²)	Q (m³/s)	QSS (Mt/year)	QST (Mt/year)	QST change (%)	Dominant Driver
Amazon	5,927,062	199,798	325.1	405.8	-6	-
Apure	137,051	2,094	16.0	18.1	-6	-
Araguaia	387,051	6,195	6.9	11.0	-6	-
Aripuanã	147,519	4,390	0.6	1.2	18*	LULCC
Beni	119,697	2,200	81.9	83.8	0	-
Bermejo	107,526	464	25.9	27.2	-31*	Precipitation
Branco	191,221	5,832	4.7	7.1	8	-
Colorado	295,416	185	0.2	0.6	-60*	Reservoir
Grande	143,928	2,277	0.5	0.6	-33*	Reservoir
Guaporé	355,220	3,315	3.9	5.4	18*	LULCC
Guaviare	139,337	6,454	10.4	14.3	4*	Precipitation
Iriri	142,686	4,563	0.6	1.1	19*	LULCC
Japurá	270,763	15,255	11.1	20.2	7	-
Juruá	182,140	5,979	29.2	34.5	-26	-
Madeira	1,372,401	28,823	155.3	172.2	-26	-
Madre de Dios	125,756	4,082	74.5	85.3	-2	-
Magdalena	261,343	7,304	28.2	38.9	-8*	LULCC
Mamoré	236,242	3,237	62.0	64.5	-7	-
Marañon	365,659	15,262	138.0	161.0	1	-
Meta	109,518	4,003	27.8	31.9	-7	-
Negro (Amazon)	716,166	34,887	9.2	14.2	10*	Precipitation
Negro (Argentina)	113,495	834	0.2	0.6	-80	-
Orinoco	940,567	33,186	116.9	151.2	-1*	Precipitation
Paraguay	535,249	2,541	6.0	8.5	-9	-
Paraná	2,602,798	21,792	59.2	65.1	-23*	Precipitation

Paranaíba	224,199	3,426	2.2	3.2	-44*	Reservoir
Parnaíba	333,763	962	1.9	3.4	-49	-
Pilcomayo	114,123	21	25.6	25.6	-2	-
Purus	379,473	11,424	24.5	33.8	9	-
Salado	226,464	175	0.3	0.9	-12*	Reservoir
San Miguel	125,840	777	2.5	2.9	7*	LULCC
São Francisco	638,874	2,779	0.9	2.6	-42*	Precipitation
Solimões	2,219,829	90,783	249.9	304.1	1	-
Tapajós	495,396	15,260	3.4	5.8	27*	LULCC
Tocantins	774,414	13,656	5.1	6.5	-46*	Reservoir
Ucayali	353,575	9,689	102.7	119.1	-4	-
Upper Paraná	954,777	15,557	5.1	6.5	-73*	Reservoir
Uruguay	267,152	7,172	4.0	4.0	-49*	Reservoir
Xingu	514,318	13,946	2.5	4.4	1*	LULCC

* Statistically significant to the level of 5% from the Mann-Kendall test.

Amazon (405 Mt/year, 48.8%), Orinoco (151 Mt/year, 18.1%), Paraná (65 Mt/year, 7.6%) and Magdalena (39 Mt/year, 4.6%) were the main SA rivers delivering sediments to the oceans (Figure 3-**a**). Comparing current and baseline periods, these rivers experienced a reduction in simulated sediment flux of 5.9%, 0.7%, 23.0%, and 7.6%, respectively. Our simulations also showed that sediment delivery to the South and North Atlantic Oceans were reduced by 26.0% and 4.7%, respectively, close to the sediment delivery reductions of the Paraná (23.0%) and Amazon (5.9%) rivers (Figure 3). The -5.0% change (Figure 3-**b**) in sediment supply to the Caribbean (69 Mt/year, 31.3%) is mainly associated with changes in the Magdalena River sediment flows.

Precipitation was the main driver responsible for reducing total simulated sediment discharge (QST) in SA rivers (Figure 2). For instance, we estimated a 6.1% decrease in the sediment delivery to the oceans for the 2011–2019 period when considering only the effect of precipitation (Fig 1-

A.4). The variable nature of precipitation over time showed that the climate driver has a widespread and important impact on sediment flux changes over large portions of SA.

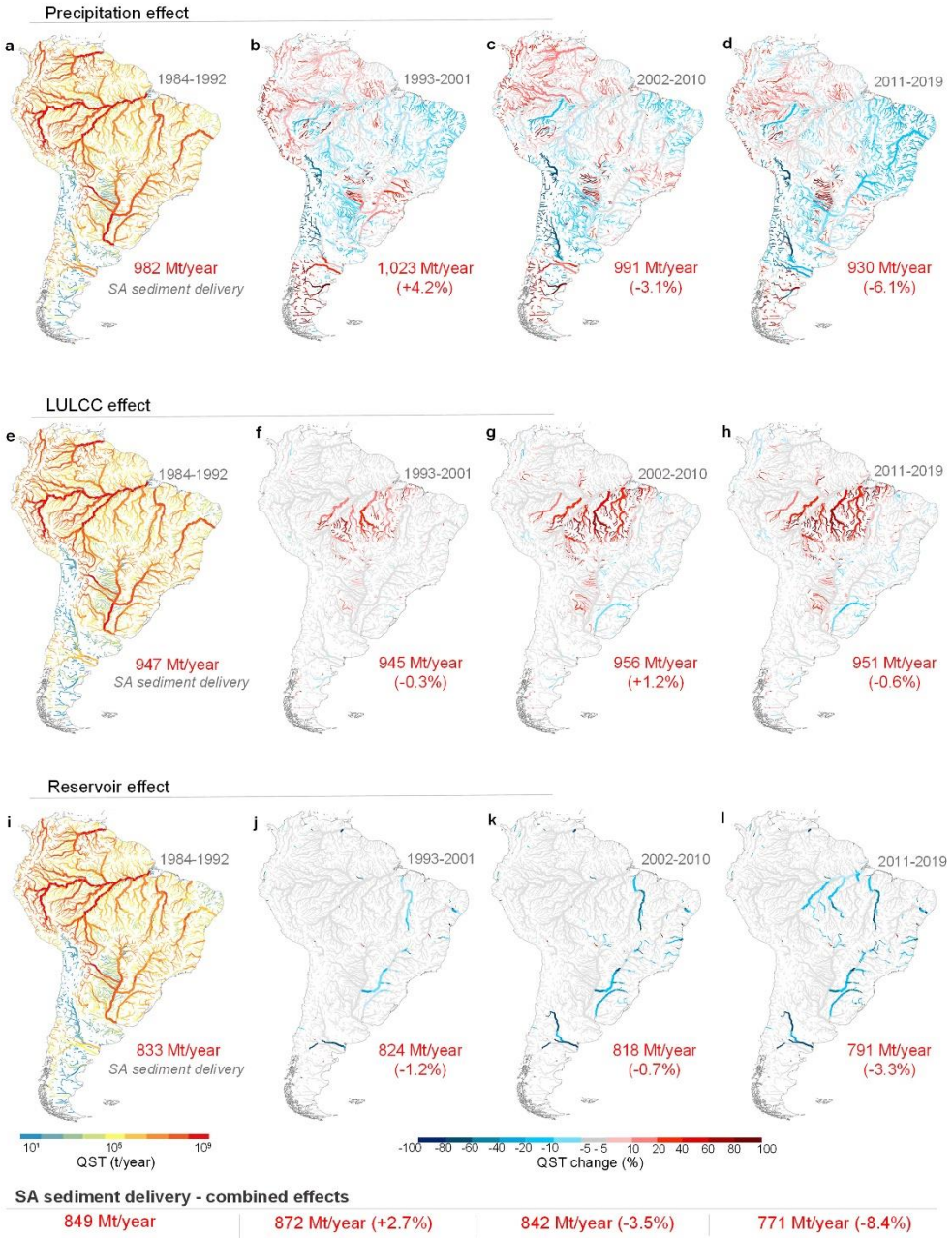

Figure 2. Temporal changes in sediment fluxes in South American rivers between 1984–2019. Maps show the QST and their changes (%) considering the isolated effect of precipitation changes (**a–d**), land use and land cover changes (LULCC, **e–h**), and existing reservoirs (**i–l**). Maps **a**, **e,** and **i** show QST values for the baseline period (1984–1992). The other maps present the sediment flow changes compared with the baseline period. Numbers in red indicate the average sediment

559 delivery from South America (SA) to the oceans in each period. Percentage values indicate the
560 increase or decrease of sediment delivery compared with the previous period. These values are
561 presented at the bottom (SA sediment delivery - combined effects) for the combined effect of
562 each driver, i.e., when simulations were performed considering the synergic effect of
563 precipitation, LULCC, and reservoirs on sediment flows.

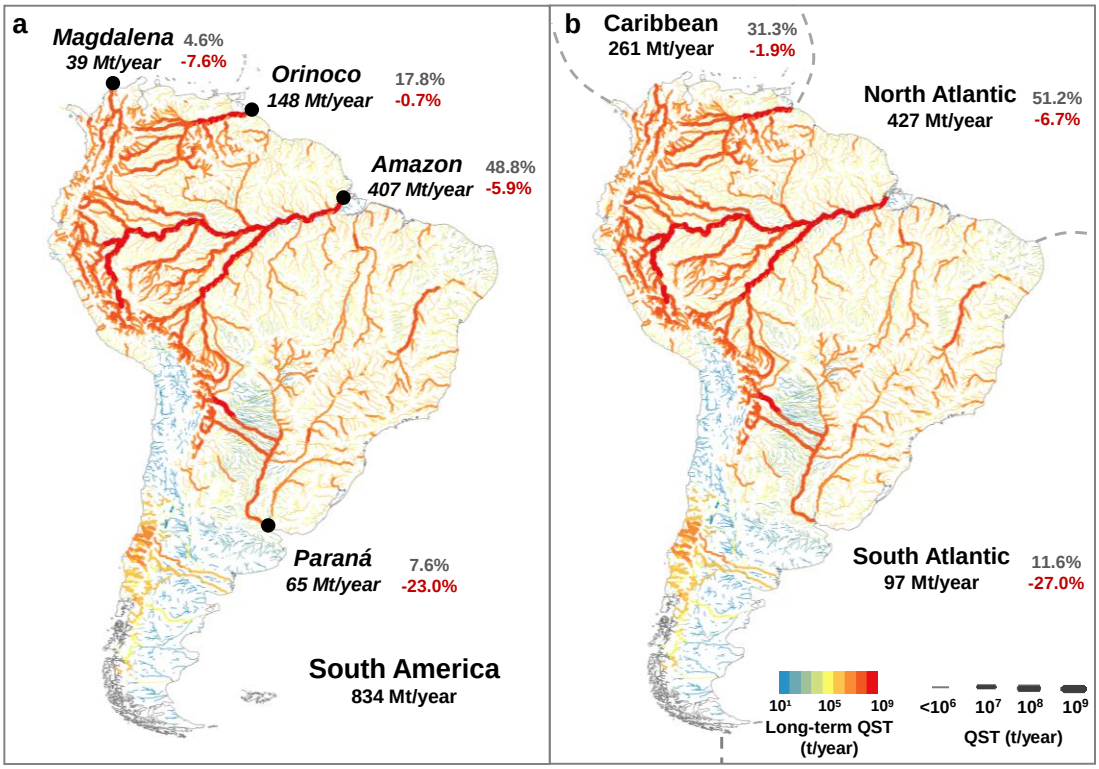

564
565 **Figure 3. Long-term average of total simulated sediment discharge (QST) and the impact in**
566 **the supply to the Caribbean, North and South Atlantic oceans**. **a**, Main rivers responsible for
567 the sediment supply to the oceans. **b**, Amount of sediment load reaching the oceans. Gray numbers
568 indicate the relative percentage of the sediment load in comparison with the total reaching the
569 oceans. Red numbers indicate the relative reduction in 2011-2019 in comparison with 1984-1992.

570 By contrast, LULCC resulted in local but more substantial effects, with several rivers showing
571 simulated QST changes above 80% (Figure 2-**h**). In addition, LULCC effects were progressive over
572 time, and the Amazon arc of the deforestation region is the main affected area (Figure 2). This
573 region has been deforested (1,424 ha/year, INPE - Instituto Nacional de Pesquisas Espaciais, 2021)
574 for livestock, soybean planting, and other crops(Song et al., 2021, 2018; Zalles et al., 2021). Since
575 1984, we observed that deforestation mostly increased the sediment flux in some Amazon sub-
576 basins such as Juruá, Japurá, Magdalena and Branco ones, as well as along the headwaters of

577 Magdalena and Orinoco rivers (Figure 2). At the same time, more significant reforestation (natural
578 or non-natural) was observed in the Uruguay River basin, in the headwaters of the Upper Paraná,
579 São Francisco, and in some small rivers on the right bank of the Paraguay River (Figure 2).

580 The effect of reservoirs was cumulative along the rivers, and greater reservoir storage capacity
581 caused more sediment retention. Sediment modeling show that from 1984 to 2010, hydropower
582 expansion le led to a greater reduction of sediment flows (as high as 80-100%) in the Tocantins,
583 Uruguay, Upper Paraná, lower São Francisco, Desaguadero, and Negro rivers (Figure 2-**k**). In the
584 last decade, hydropower expansion has largely affected the Amazon region (Fig 2-**l**), resulting in a
585 significant change in the sediment flows in this region. By comparing the current (2011–2019) and
586 baseline (1984–1992) periods, river impoundments were responsible for a 5% reduction in total
587 sediment delivery to the oceans. Several reservoirs were built for the Brazilian hydropower
588 expansion, especially after its energy crisis at the beginning of the 21st century. However, many
589 dams existed in SA rivers before 1984 (Figure 1). We found a 25% reduction in sediment delivery
590 to the oceans caused by the reservoirs operating in 2019 compared with a scenario without
591 reservoirs (Figure 4). It is well known that sediment trapping in reservoir lakes can induce
592 downstream sediment erosion, but in general, the sediment volume trapped upstream greatly
593 overcomes the sediment volume eroded in downstream.

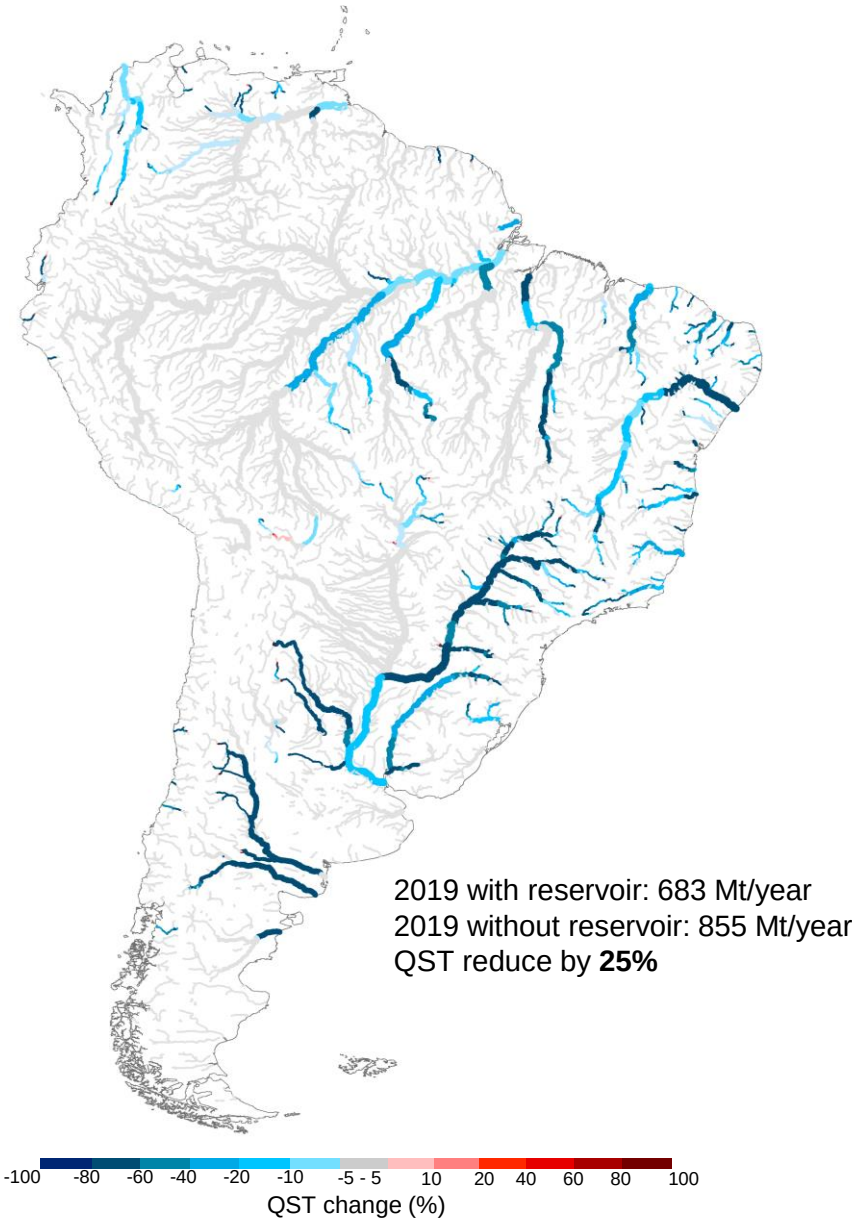

Figure 4. QST change due to reservoir effect considering the year of 2019. Two simulations were performed: one with presence and other with absence of the 234 large reservoirs presented in Extended Data Figure 1. These changes indicate not only the effect of reservoir in the simulated period but also those one existing before 1984.

The main hotspots for simulated QST increases driven by LULCC and precipitation were in the Amazon region (Figure 5). These sediment flow disturbances can require more fertilizers (Borrelli et al., 2017) for food production, affecting the meander migration and generating social and

602 economic damage to riverine communities (Nagel et al., 2022). Increases in Amazon sediment
603 flows can also be accompanied by higher mercury concentrations in rivers (Benefice et al., 2010;
604 Webb et al., 2004; Yokoo et al., 2003), wetlands (Roulet et al., 2001) and fishes (Lino et al., 2019).
605 These increases can be related to changes in the neurobehavioral capacities of adults observed in
606 parts of Brazil, Ecuador, and Bolivia (Benefice et al., 2010; Webb et al., 2004; Yokoo et al., 2003).

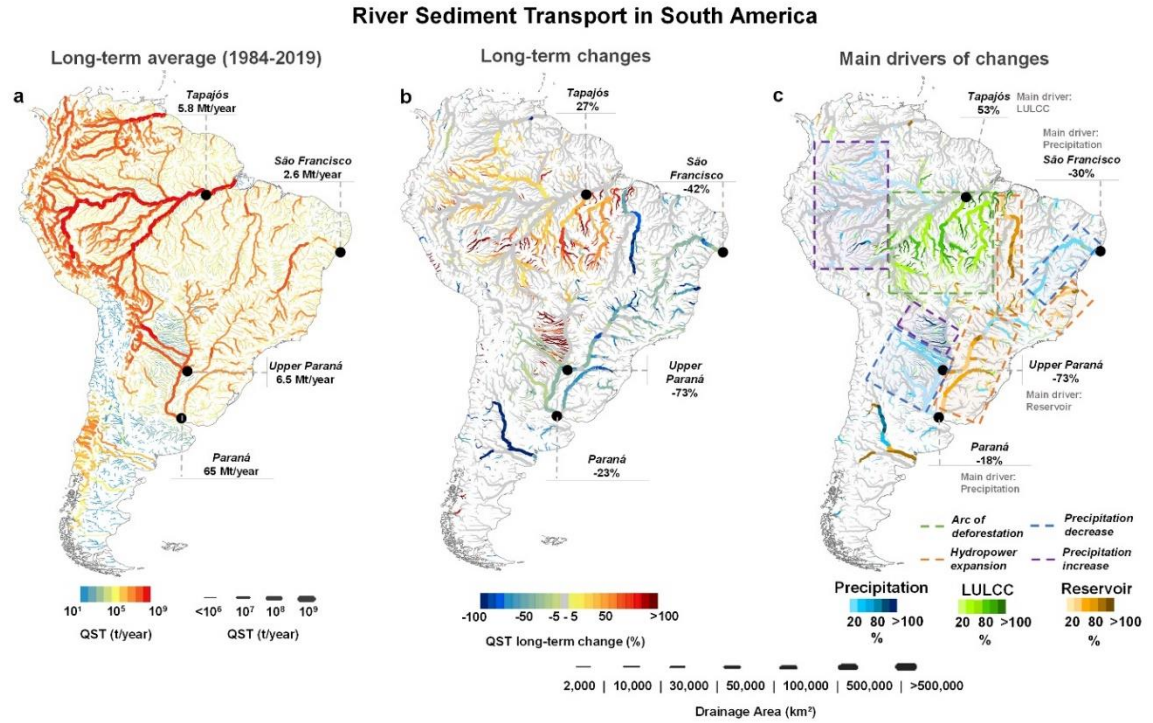

607
608 **Figure 5. Spatial overview of trends, magnitude, and main drivers of changes in sediment**
609 **transport of South American rivers between 1984-2019. a**) map of the long-term average of total
610 simulated sediment discharge (QST) considering the precipitation and human-induced changes by
611 land use and land cover changes (LULCC) and reservoirs constructions. **b**) Statistically significant
612 QST long-term changes to the level of 5% considering the Mann Kendall test (M-K test). **c**)
613 Magnitude of sediment flow changes considering the main driver (precipitation, LULCC, or
614 reservoir) in each river reach. Hotspots of changes are highlighted in rectangles. For example, it is
615 observed that Tapajós River transported 5.8 Mt/year on average from 1984-2019, with an
616 increasing trend of 27%, in which the LULCC (main) driver was responsible for an increase of 53%.

617 Over time, the implementation of many reservoirs caused substantial simulated QST reductions
618 (> 50%) in the Tocantins, Upper Paraná, Uruguay, and Lower São Francisco rivers (Figure 5-**c**).
619 Ecological and geomorphological implications have already been reported for some of these rivers

620 (Bandeira et al., 2013; da Silva et al., 2020; Maavara et al., 2015). Lower sediment supply to
621 downstream reservoirs can lead to the loss of riparian vegetation, affecting the water quality,
622 local biodiversity (Naiman et al., 1993), and other wetland vegetation species (Swanson and
623 Bohlman, 2021). Reduced sediment flows can also lead to fewer nutrients and decreased fishery
624 yields, as reported for the São Francisco (Cavali et al., 2020) and Paraná (Maavara et al., 2015)
625 rivers. Hydropower expansion has recently reached the Amazon region, resulting in a statistically
626 significant change in sediment flows. By comparing pre- and post-construction of Santo Antônio
627 and Jirau dams, we estimated a 43% decline in the Madeira River's QST. This remarkable change
628 affected the Amazon River, which experienced a 19% reduction in sediment load over the same
629 period. The coastal region between the mouths of the Amazon and Orinoco rivers is the largest
630 mud beach complex on Earth (Anthony et al., 2014), and may be seriously affected by substantial
631 reductions in sediment supply by Amazon River (Forsberg et al., 2017; Latrubesse et al., 2017).
632 This reduction could also affect the ability of mangroves to act as a carbon sink. These forests
633 account for approximately 10–15% of total carbon sequestration while covering only around 0.5%
634 of the total global coastal area (Ezcurra et al., 2019).

635 Regarding the impacts on simulated QST from precipitation decreases, the most significant
636 changes were found in the Bermejo River (-31%). This river provides approximately 90% of the
637 Lower Paraná sediment load (Amsler and Drago, 2009), playing a major role in maintaining its
638 ecosystems (Thorp et al., 2006). Climate change projections (Figure S1 - Supporting Information
639 S1) suggest that the Bermejo River will likely experience average precipitation and river discharge
640 reductions in the future. Consequently, the sediment supply to the Lower Paraná River is expected
641 to decline, increasing the vulnerability of the ecosystems that depend on it.

642 **4.3 Implications for the ecosystem, water, and land management**

643 When sediment flows are changing, other aspects of the environment can also be affected. In
644 South America, planned reservoirs (Figure S1 - Supporting Information S1) are particularly
645 concerning, especially those in the Pantanal and Amazon basin. Even if only some of them are
646 built, irreversible environmental consequences could occur (Forsberg et al., 2017). Sediments
647 from uplands carried to the Pantanal wetlands support geomorphological dynamics, wildlife
648 habitats, and biological productivity. However, existing reservoirs have reduced the sediment
649 supply by around 20% in these environments (Fantin-Cruz et al., 2020 and Figure 5). In addition,
650 Andean reservoirs can dramatically change the sediment and nutrient inflows to the Amazon
651 rivers and floodplains and the North Atlantic Ocean. An earlier study showed that six planned
652 dams accounting for only 7% of the total drainage area of the Amazon Basin could reduce the
653 basin-wide sediment supply by 64% (Forsberg et al., 2017).

654 Both increasing changes in simulated QST due to LULCC or precipitation changes in SA require
655 measures to minimize their impacts. From our results, hotspots include the Amazon, where
656 efforts should focus on reducing deforestation. However, the Brazilian Cerrado, Caatinga, Atlantic
657 Rainforest, and Pampa biomes were also severely degraded in the past and would benefit
658 significantly from erosion control practices. Our results can assist in the delineation of ecosystem
659 restoration strategies by identifying the main areas needing recovery (Zalles et al., 2021), through
660 policies such as payment for ecosystem services, for example (Latrubesse et al., 2019; Song et al.,
661 2018). Sustainable agriculture by farmers must be encouraged, providing practices aimed at soil
662 erosion reduction and improving both terrestrial and aquatic ecosystems quality (Borrelli et al.,
663 2017). Concerning mercury impacts associated with deforestation, consider that (i) Brazilian
664 Amazon riverine populations have a per capita fish consumption of up to 94 kg/year, which is 5.8

665 times the world average (Isaac and de Almeida, 2011), and (ii) our results showed that QST
666 increase rates reached more than 80%. Therefore, the creation of programs and actions to
667 monitor fishes and prevent damage to the health of the riverine population, such as providing
668 solutions and better diet alternatives (Benefice et al., 2010), is also important.

669 Although dams can cause several negative impacts on sediment flows and ecosystems, they also
670 have contributed to worldwide water and energy security, supporting economic and social
671 development (Hogeboom et al., 2018; Tilmant et al., 2014). In 2018, reservoirs used for
672 hydropower generation, irrigation, industrial and domestic water supply, flood protection, fishing,
673 and recreation were valued at US$265 billion per year (Hogeboom et al., 2018). Because of these
674 factors, trade-offs and the adoption of sustainable management practices in reservoir operation
675 are essential (Best, 2019), including for major areas requiring new dam construction, such as the
676 Amazon and Pantanal (Randle et al., 2021). Such practices would permit sediment passage
677 through reservoirs to provide environmental benefits (Randle et al., 2021) and minimize
678 environmental impacts.

679 5 Conclusions

680 Sediment flow changes in SA induced by human activities such as deforestation and river
681 damming are a consequence of demands from local populations and other. Both increases and
682 decreases in sediment flows can be problematic for the environment and society because each
683 ecosystem is unique. Thus, in this study we aimed to comprehend the spatiotemporal changes in
684 sediment fluxes in SA over the last 36 years (1984-2019). We found that 51% of the main SA rivers
685 experienced statistically significant changes in simulated sediment transport over this period, with
686 36% due to Amazon deforestation and river damming and 15% due to precipitation changes. We
687 also estimated a 10% reduction in the average sediment delivery to the oceans.

688 Amazon, Orinoco, Paraná and Magdalena were the main SA rivers delivering sediments to the
689 oceans, and these rivers experienced a reduction in simulated sediment flux of 5.9%, 0.7%, 23.0%,
690 and 7.6%, respectively. Precipitation was the main driver responsible for reducing total simulated
691 sediment discharge (QST) in SA rivers. By contrast, LULCC resulted in local but more substantial
692 effects, with several rivers showing simulated QST changes above 80%. Similarly, to LULCC,
693 hydropower expansion led to a greater reduction of sediment flows (as high as 80-100%) in the
694 Tocantins, Uruguay, Upper Paraná, lower São Francisco, Desaguadero, and Negro rivers. Our
695 results of simulation also show that Amazon region is the most affected one due to deforestation,
696 and, especially in the last decade, also by reservoirs.

697 Our study is the first to provide a thorough and consistent analysis of the synergistic effects of
698 LULCC, river damming, and precipitation change on sediment flows for the entire SA continent
699 from 1984 to 2019. Our modeling outputs provide unprecedented information about the status
700 of sediment dynamics in SA, and a means to develop evidence-based strategies and
701 transboundary policies related to continental-wide sediment dynamics and the conservation and
702 restoration of ecosystems. This understanding of the evolution of sediment flow changes across
703 space and time can help mitigate impacts on people and nature, based on our identification of
704 the most sediment-affected regions. The approach used here can also be useful as described next
705 for applications in other locations. Furthermore, the findings and data provided in this study may
706 be useful in future investigations of carbon fluxes, nutrient transport, biological productivity,
707 human food and energy safety, and other studies related to ecosystem maintenance and soil
708 conservation.

709 The MGB-SED AS model has shown ability to properly simulate sediment fluxes in several sites of
710 South America. However, large-scale modeling is not free of uncertainties, which requires that

711 the results and conclusions be understand from this perspective. In the future, we intend to
712 perform sensitivity/uncertainties analyses to improve our knowledge about continental sediment
713 modeling, which also constitutes part of our continental modeling research agenda, started with
714 the work of Siqueira et al. (2018). Future works could also use different methods and approaches
715 to represent other processes like gully and lateral erosions; different particle sizes distribution;
716 new schemes for dam operation. In addition, the model could be updated and re-calibrated using
717 new databases of soil, land use, climate and precipitation data.

718 Acknowledgments

719 H.O.F. and F.M.F. thanks the Brazilian CNPq (Conselho Nacional de Desenvolvimento Científico e
720 Tecnológico) for supporting this research under the Grants Number 167867/2018-0 and
721 305636/2019-7. P.B. was funded by the EcoSSSoil Project, Korea Environmental Industry &
722 Technology Institute (KEITI), Korea (Grant No. 2019002820004). This study was financed in part
723 by the Coordenação de Aperfeiçoamento de Pessoal de Nível Superior - Brasil (CAPES) - Finance
724 Code 001.

725 Data availability

726 Data supporting the findings of this study are available in the references cited in the main text,
727 methods, and Supporting Information S1. Also, any data can be provided from the corresponding
728 author upon reasonable request. Simulated Suspended Sediment Discharge for South America
729 Rivers (MGB-SED AS) - V2.0 dataset is available in: doi.org/10.17632/ncr6d42tx5.1. This dataset
730 provides both annual long-term average and daily simulated data. More information and datasets
731 can be found in https://www.ufrgs.br/samewater/.
732

Code availability

The source code of the MGB-SED AS model is available at https://www.ufrgs.br/samewater/produtos/south-america-sediment-model/

6 References

Alarcón, J.J., Szupiany, R., Montagnini, M.D., Gaudin, H., Prendes, H.H., Amsler, M.L., 2003. Evaluación del transporte de sedimentos en el tramo medio del Río Paraná, in: Primer Simposio Regional Sobre Hidráulica de Ríos. Ezeiza.

Albert, J.S., Destouni, G., Duke-Sylvester, S.M., Magurran, A.E., Oberdorff, T., Reis, R.E., Winemiller, K.O., Ripple, W.J., 2021. Scientists' warning to humanity on the freshwater biodiversity crisis. Ambio 50, 85–94. https://doi.org/10.1007/s13280-020-01318-8

Almagro, A., Oliveira, P.T.S., Nearing, M.A., Hagemann, S., 2017. Projected climate change impacts in rainfall erosivity over Brazil. Sci Rep 7, 1–12. https://doi.org/10.1038/s41598-017-08298-y

Amsler, M.L., Drago, E.C., 2009. A review of the suspended sediment budget at the confluence of the Paran´a and Paraguay Rivers. Hydrological Processes: An International Journal 23, 3230–3235. https://doi.org/10.1002/hyp

Andreadis, K.M., Schumann, G.J.P., Pavelsky, T., 2013. A simple global river bankfull width and depth database. Water Resouces Research.

Anthony, E.J., Gardel, A., Gratiot, N., 2014. Fluvial sediment supply, mud banks, cheniers and the morphodynamics of the coast of South America between the Amazon and Orinoco river mouths. Geol Soc Spec Publ 388, 533–560. https://doi.org/10.1144/SP388.8

Bandeira, J.V., Farias, E. de G.G., Lorenzzetti, J.A., Salim, L.H., 2013. Resposta morfológica da foz do rio São Francisco, devido à retenção de sedimentos nos reservatórios. Vetor 23, 5–17.

Barbarossa, V., Schmitt, R.J.P., Huijbregts, M.A.J., Zarfl, C., King, H., Schipper, A.M., 2020. Impacts of current and future large dams on the geographic range connectivity of freshwater fish worldwide. Proc Natl Acad Sci U S A 117, 3648–3655. https://doi.org/10.1073/pnas.1912776117

Bates, P.D., Horritt, M.S., Fewtrell, T.J., 2010. A simple inertial formulation of the shallow water equations for efficient two-dimensional flood inundation modelling. J Hydrol (Amst) 387, 33–45. https://doi.org/10.1016/j.jhydrol.2010.03.027

Beck, H.E., van Dijk, A.I.J.M., de Roo, A., Dutra, E., Fink, G., Orth, R., Schellekens, J., 2017. Global evaluation of runoff from 10 state-of-the-art hydrological models. Hydrol Earth Syst Sci 21, 2881–2903.

766 Beighley, R.E., Gummadi, V., 2011. Developing channel and floodplain dimensions with limited
767 data: A case study in the Amazon Basin. Earth Surf Process Landf 36, 1059–1071.

768 Benavidez, R., Jackson, B., Maxwell, D., Norton, K., 2018. A review of the (Revised) Universal Soil
769 Loss Equation ((R)USLE): With a view to increasing its global applicability and improving soil
770 loss estimates. Hydrol Earth Syst Sci 22, 6059–6086. https://doi.org/10.5194/hess-22-
771 6059-2018

772 Benefice, E., Luna-Monrroy, S., Lopez-Rodriguez, R., 2010. Fishing activity, health characteristics
773 and mercury exposure of Amerindian women living alongside the Beni River (Amazonian
774 Bolivia). Int J Hyg Environ Health 213, 458–464.
775 https://doi.org/10.1016/j.ijheh.2010.08.010

776 Best, J., 2019. Anthropogenic stresses on the world's big rivers. Nat Geosci 12, 7–21.
777 https://doi.org/10.1038/s41561-018-0262-x

778 Borrelli, P., Robinson, D.A., Fleischer, L.R., Lugato, E., Ballabio, C., Alewell, C., Meusburger, K.,
779 Modugno, S., Schütt, B., Ferro, V., Bagarello, V., Oost, K. van, Montanarella, L., Panagos, P.,
780 2017. An assessment of the global impact of 21st century land use change on soil erosion.
781 Nat Commun 8, 1–13. https://doi.org/10.1038/s41467-017-02142-7

782 Bozkurt, D., Rondanelli, R., Garreaud, R., 2016. Impact of Warmer Eastern Tropical Pacific SST on
783 the March 2015 Atacama Floods. American Meteorological Society 144, 4441–4460.
784 https://doi.org/10.1175/MWR-D-16-0041.s1

785 Buarque, D.C., 2015. Simulação da geração e do transporte de sedimetnos em grandes bacias:
786 estudo de caso do rio Madeira. Universidade Federal do Rio Grande do Sul, Porto Alegre,
787 Tese (Doutorado em Recursos Hídricos e Saneamento Ambiental).

788 Cai, W., McPhaden, M.J., Grimm, A.M., Rodrigues, R.R., Taschetto, A.S., Garreaud, R.D., Dewitte,
789 B., Poveda, G., Ham, Y.G., Santoso, A., Ng, B., Anderson, W., Wang, G., Geng, T., Jo, H.S.,
790 Marengo, J.A., Alves, L.M., Osman, M., Li, S., Wu, L., Karamperidou, C., Takahashi, K., Vera,
791 C., 2020. Climate impacts of the El Niño–Southern Oscillation on South America. Nat Rev
792 Earth Environ. https://doi.org/10.1038/s43017-020-0040-3

793 Carvalho, T.M., 2009. Avaliação do transporte de carga sedimentar no médio rio Araguaia.
794 Geosul 24, 147–160.

795 Cavali, J., Mojica, A.B., Filho, J.V.D., 2020. Percepção dos pescadores sobre as mudanças no
796 baixo rio São Francisco, in: Soares, E.C., Silva, J.V., Navas, R. (Eds.), O Baixo São Francisco:
797 Características Ambientais e Sociais. Edufal, Maceió-AL.

798 CNEN/CDTN - Centro de Desenvolvimento da Tecnologia Nuclear, IFNMG/Campus Januária -
799 Instituto Federal do Norte de Minas Gerais, 2020. Caracterização Qualitativa e Quantitativa
800 de Parâmetros Hídricos e Sedimentológicos da Rede de Drenagem do Rio Pandeiros. Belo
801 Horizonte.

802 Cohen, S., Kettner, A.J., Syvitski, J.P.M., 2014. Global suspended sediment and water discharge
803 dynamics between 1960 and 2010: Continental trends and intra-basin sensitivity. Glob
804 Planet Change 115, 44–58. https://doi.org/10.1016/j.gloplacha.2014.01.011

805 Cohen, S., Kettner, A.J., Syvitski, J.P.M., Fekete, B.M., 2013. WBMsed, a distributed global-scale
806 riverine sediment flux model: Model description and validation. Comput Geosci 53, 80–93.
807 https://doi.org/10.1016/j.cageo.2011.08.011

808 Collischonn, W., Allasia, D., da Silva, B.C., Tucci, C.E.M., 2007. The MGB-IPH model for large-scale
809 rainfall-runoff modelling. Hydrological Sciences Journal 52, 878–895.
810 https://doi.org/10.1623/hysj.52.5.878

811 Costanza, R., de Groot, R., Farberll, S., Grassot, M., Hannon, B., Limburg, K., Naeem, S., O, R. v,
812 Paruelo, J., Raskin, R.G., Suttonllll, P., 1997. The value of the world's ecosystem services
813 and natural capital. Nature 387, 253–260.
814 https://doi.org/https://doi.org/10.1038/387253a0

815 da Silva, I.G., Pelicice, F.M., Rodrigues, L.C., 2020. Loss of phytoplankton functional and
816 taxonomic diversity induced by river regulation in a large tropical river. Hydrobiologia 847,
817 3471–3485. https://doi.org/10.1007/s10750-020-04355-2

818 Dethier, E.N., Renshaw, C.E., Magilligan, F.J., 2022. Rapid changes to global river suspended
819 sediment flux by humans. Science (1979) 376, 1447–1452.

820 Diodato, N., Filizola, N., Borrelli, P., Panagos, P., Bellocchi, G., 2020. The rise of climate-driven
821 sediment discharge in the amazonian river basin. Atmosphere (Basel) 11.
822 https://doi.org/10.3390/atmos11020208

823 Dissanayake, C.B., Chandrajith, R., 2009. Phosphate Mineral Fertilizers, trace metals and human
824 health. J Natl Sci Found. https://doi.org/10.4038/jnsfsr.v37i3.1219

825 Doetterl, S., van Oost, K., Six, J., 2012. Towards constraining the magnitude of global agricultural
826 sediment and soil organic carbon fluxes. Earth Surf Process Landf 37, 642–655.
827 https://doi.org/10.1002/esp.3198

828 Dunn, F.E., Darby, S.E., Nicholls, R.J., Cohen, S., Zarfl, C., Fekete, B.M., 2019. Projections of
829 declining fluvial sediment delivery to major deltas worldwide in response to climate
830 change and anthropogenic stress. Environmental Research Letters 14, 084034.
831 https://doi.org/10.1088/1748-9326/ab304e

832 Ezcurra, E., Barrios, E., Ezcurra, P., Ezcurra, A., Vanderplank, S., Vidal, O., Villanueva-Almanza, L.,
833 Aburto-Oropeza, O., 2019. A natural experiment reveals the impact of hydroelectric dams
834 on the estuaries of tropical rivers. Sci. Adv 5, 9875–9888.
835 https://doi.org/10.1126/sciadv.aau9875

836 Fagundes, H. de O., Fan, F.M., Paiva, R.C.D., 2019. Automatic calibration of a large-scale
837 sediment model using suspended sediment concentration, water quality, and remote
838 sensing data. Brazilian Journal of Water Resources 24, 1–18. https://doi.org/10.1590/2318-
839 0331.241920180127

840 Fagundes, H.O., Fan, F.M., Paiva, R.C.D., Siqueira, V.A., Buarque, D.C., Kornowski, L.W., Laipelt,
841 L., Collischonn, W., 2021. Sediment Flows in South America Supported by Daily Hydrologic-
842 Hydrodynamic Modeling. Water Resour Res 57. https://doi.org/10.1029/2020WR027884

Fagundes, H.O., Paiva, R.C.D., Fan, F.M., Buarque, D.C., Fassoni-Andrade, A.C., 2020. Sediment modeling of a large-scale basin supported by remote sensing and in-situ observations. Catena (Amst) 190, 104535. https://doi.org/10.1016/j.catena.2020.104535

Fan, F.M., Buarque, D.C., Pontes, P.R.M., Collischonn, W., 2015. Um Mapa de Unidades de Resposta Hidrológica para a América do Sul. XXI Simpósio Brasileiro e Recursos Hídricos 1–8.

Fan, F.M., Siqueira, V.A., Fleischmann, A.S., Brêda, J.P.F., de Paiva, R.C.D., Pontes, P.R.M., Collischonn, W., 2021a. On the discretization of river networks for large scale hydrologic-hydrodynamic models. Revista Brasileira de Recursos Hidricos 26. https://doi.org/10.1590/2318-0331.262120200070

Fan, F.M., Siqueira, V.A., Fleischmann, A.S., Brêda, J.P.F., de Paiva, R.C.D., Pontes, P.R.M., Collischonn, W., 2021b. On the discretization of river networks for large scale hydrologic-hydrodynamic models. Revista Brasileira de Recursos Hidricos 26. https://doi.org/10.1590/2318-0331.262120200070

Fantin-Cruz, I., de Oliveira, M.D., Campos, J.A., de Campos, M.M., de Souza Ribeiro, L., Mingoti, R., de Souza, M.L., Pedrollo, O., Hamilton, S.K., 2020. Further Development of Small Hydropower Facilities Will Significantly Reduce Sediment Transport to the Pantanal Wetland of Brazil. Front Environ Sci 8. https://doi.org/10.3389/fenvs.2020.577748

FAO/UNESCO, 1974. FAO/UNESCO Soil Map of the World | Food and Agriculture Organization of the United Nations [WWW Document]. FAO/UNESCO Soil Map of the World.

Fassoni-Andrade, A.C., Paiva, R.C.D. de, 2019. Mapping spatial-temporal sediment dynamics of river-floodplains in the Amazon. Remote Sens Environ 221, 94–107. https://doi.org/10.1016/j.rse.2018.10.038

Filho, O.S., 2016. Monitoramento hidrossedimentométrico e avaliação de métodos de cálculo de descarga sólida total no rio Vacacaí Mirim (Dissertação). Universidade Federal de Santa Maria, Santa Maria.

Fleischmann, A., Collischonn, W., Paiva, R., Tucci, C.E., 2019a. Modeling the role of reservoirs versus floodplains on large-scale river hydrodynamics. Natural Hazards 99, 1075–1104. https://doi.org/10.1007/s11069-019-03797-9

Fleischmann, A., Paiva, R., Collischonn, W., 2019b. Can regional to continental river hydrodynamic models be locally relevant? A cross-scale comparison. J Hydrol X 3, 100027. https://doi.org/10.1016/j.hydroa.2019.100027

Fleischmann, A., Siqueira, V., Paris, A., Collischonn, W., Paiva, R., Pontes, P., Crétaux, J.F., Bergé-Nguyen, M., Biancamaria, S., Gosset, M., Calmant, S., Tanimoun, B., 2018. Modelling hydrologic and hydrodynamic processes in basins with large semi-arid wetlands. J Hydrol (Amst) 561, 943–959. https://doi.org/10.1016/j.jhydrol.2018.04.041

Fleischmann, A.S., Brêda, J.P.F., Passaia, O.A., Wongchuig, S.C., Fan, F.M., Paiva, R.C.D., Marques, G.F., Collischonn, W., 2021. Regional scale hydrodynamic modeling of the river-

floodplain-reservoir continuum. J Hydrol (Amst) 596. https://doi.org/10.1016/j.jhydrol.2021.126114

Föeger, L.B., Buarque, D.C., Pontes, P.R.M., Fagundes, H. de O., Fan, F.M., 2022. Large-scale sediment modeling with inertial flow routing: Assessment of Madeira river basin. Environmental Modelling and Software 149. https://doi.org/10.1016/j.envsoft.2022.105332

Forsberg, B.R., Melack, J.M., Dunne, T., Barthem, R.B., Goulding, M., Paiva, R.C.D., Sorribas, M. v., Silva, U.L., Weisser, S., 2017. The potential impact of new Andean dams on Amazon fluvial ecosystems, PLoS ONE. https://doi.org/10.1371/journal.pone.0182254

Gamaro, P.E.M., Maldonado, L.H., Castro, J.L., 2014. APLICAÇÃO DO MÉTODO DAS DUNAS PARA DETERMINAÇÃO DA DESCARGA DE FUNDO NO RIO PARANÁ, in: Anais Do XI Encontro Nacional de Engenharia de Sedimentos. João Pessoa.

Gamaro, P.E.M., Maldonado, L.H., Lima, K.A., 2011. AVALIAÇÃO DA CARGA DE SEDIMENTOS DE FUNDO PELO MÉTODO DE DESLOCAMENTO DE DUNAS E MEDIDORES ACÚSTICOS DOPPLER, in: Anais Do XIX Simpósio Brasileiro de Recursos Hídricos. Maceió.

Getirana, A., Peters-Lidard, C., Rodell, M., Bates, P.D., 2017. Trade-off between cost and accuracy in large-scale surface water dynamic modeling. Water Resour Res 53, 4942–4955. https://doi.org/10.1002/2017WR020519

González, M.H., Murgida, A.M., 2012. 7 Seasonal Summer Rainfall Prediction in Bermejo River Basin in Argentina, in: Hannachi, A. (Ed.), Climate Variability—Some Aspects, Challenges and Prospects. InTech, pp. 141–160.

Grill, G., Lehner, B., Thieme, M., Geenen, B., Tickner, D., Antonelli, F., Babu, S., Borrelli, P., Cheng, L., Crochetiere, H., Ehalt Macedo, H., Filgueiras, R., Goichot, M., Higgins, J., Hogan, Z., Lip, B., McClain, M.E., Meng, J., Mulligan, M., Nilsson, C., Olden, J.D., Opperman, J.J., Petry, P., Reidy Liermann, C., Sáenz, L., Salinas-Rodríguez, S., Schelle, P., Schmitt, R.J.P., Snider, J., Tan, F., Tockner, K., Valdujo, P.H., van Soesbergen, A., Zarfl, C., 2019. Mapping the world's free-flowing rivers. Nature 569, 215–221. https://doi.org/10.1038/s41586-019-1111-9

Hanasaki, N, Kanae, S., Oki, T., 2006. A reservoir operation scheme for global river routing models. J Hydrol (Amst) 327, 22–41.

Hanasaki, Naota, Kanae, S., Oki, T., 2006. A reservoir operation scheme for global river routing models. J Hydrol (Amst) 327, 22–41. https://doi.org/10.1016/j.jhydrol.2005.11.011

Hogeboom, R.J., Knook, L., Hoekstra, A.Y., 2018. The blue water footprint of the world's artificial reservoirs for hydroelectricity, irrigation, residential and industrial water supply, flood protection, fishing and recreation. Adv Water Resour 113, 285–294. https://doi.org/10.1016/j.advwatres.2018.01.028

Huang, C., Zhou, Z., Teng, M., Wu, C., Wang, P., 2020. Effects of climate, land use and land cover changes on soil loss in the Three Gorges Reservoir area, China. Geography and Sustainability 1, 200–208. https://doi.org/10.1016/j.geosus.2020.08.001

INPE - Instituto Nacional de Pesquisas Espaciais, 2021. TerraBrasilis. PRODES (Desmatamento). Taxas de desmatamento acumulado. http://www.obt.inpe.br/OBT/assuntos/programas/amazonia/prodes/citacoes-ao-prodes.

Isaac, V.J., de Almeida, M.C., 2011. El consumo de pescado en La Amazonía Brasileña. Rome.

Julien, P.Y., 2010. Erosion and Sedimentation, Second. ed. Cambridge University Press, New York.

Kemppinen, K.M.S., Collins, P.M., Hole, D.G., Wolf, C., Ripple, W.J., Gerber, L.R., 2020. Global reforestation and biodiversity conservation. Conservation Biology 34, 1221–1228. https://doi.org/10.1111/cobi.13478

Kendall, M.G., Gibbons, J.D., 1975. Rank correlation methods. Griffin, London.

Kouwen, N., Soulis, E.D., Pietroniro, A., Donald, J., HARRINGTON; R. A, 1993. Grouped Response Units for Distributed Hydrologic Modeling. J Water Resour Plan Manag 119, 289–305.

Latosinski, F.G., Szupiany, R.N., Guerrero, M., Amsler, M.L., Vionnet, C., 2017. The ADCP's bottom track capability for bedload prediction: Evidence on method reliability from sandy river applications. Flow Measurement and Instrumentation 54, 124–135. https://doi.org/10.1016/j.flowmeasinst.2017.01.005

Latrubesse, E.M., Amsler, M.L., de Morais, R.P., Aquino, S., 2009. The geomorphologic response of a large pristine alluvial river to tremendous deforestation in the South American tropics: The case of the Araguaia River. Geomorphology 113, 239–252. https://doi.org/10.1016/j.geomorph.2009.03.014

Latrubesse, E.M., Arima, E., Ferreira, M.E., Nogueira, S.H., Wittmann, F., Dias, M.S., Dagosta, F.C.P., Bayer, M., 2019. Fostering water resource governance and conservation in the Brazilian Cerrado biome. Conserv Sci Pract 1. https://doi.org/10.1111/csp2.77

Latrubesse, E.M., Arima, E.Y., Dunne, T., Park, E., Baker, V.R., D'Horta, F.M., Wight, C., Wittmann, F., Zuanon, J., Baker, P.A., Ribas, C.C., Norgaard, R.B., Filizola, N., Ansar, A., Flyvbjerg, B., Stevaux, J.C., 2017. Damming the rivers of the Amazon basin. Nature 546, 363–369. https://doi.org/10.1038/nature22333

Latrubesse, E.M., Stevaux, J.C., Sinha, R., 2005. Tropical rivers. Geomorphology 70, 187–206. https://doi.org/10.1016/j.geomorph.2005.02.005

Lehner, B., Verdin, K., Jarvis, A., 2008. New global hydrography derived from spaceborne elevation data. Eos (Washington DC) 89, 93–94. https://doi.org/https://doi.org/10.1029/2008EO100001

Li, L., Ni, J., Chang, F., Yue, Y., Frolova, N., Magritsky, D., Borthwick, A.G.L., Ciais, P., Wang, Y., Zheng, C., Walling, D.E., 2020. Global trends in water and sediment fluxes of the world's large rivers. Sci Bull (Beijing) 65, 62–69. https://doi.org/10.1016/j.scib.2019.09.012

Lino, A.S., Kasper, D., Guida, Y.S., Thomaz, J.R., Malm, O., 2019. Total and methyl mercury distribution in water, sediment, plankton and fish along the Tapajós River basin in the

957 Brazilian Amazon. Chemosphere 235, 690–700.
958 https://doi.org/10.1016/j.chemosphere.2019.06.212

959 Maavara, T., Parsons, C.T., Ridenour, C., Stojanovic, S., Dürr, H.H., Powley, H.R., van Cappellen,
960 P., 2015. Global phosphorus retention by river damming. Proc Natl Acad Sci U S A 112,
961 15603–15608. https://doi.org/10.1073/pnas.1511797112

962 Macklin, M.G., Lewin, J., 2019. River stresses in anthropogenic times: Large-scale global patterns
963 and extended environmental timelines. Prog Phys Geogr 43, 3–23.
964 https://doi.org/10.1177/0309133318803013

965 Marengo, J.A., Galdos, M. v., Challinor, A., Cunha, A.P., Marin, F.R., Vianna, M. dos S., Alvala,
966 R.C.S., Alves, L.M., Moraes, O.L., Bender, F., 2022. Drought in Northeast Brazil: A review of
967 agricultural and policy adaptation options for food security. Climate Resilience and
968 Sustainability 1. https://doi.org/10.1002/cli2.17

969 Martins, D.P., Bravard, J.-P., Stevaux, J.C., 2009. Dynamics of water flow and sediments in the
970 Upper Paraná River between Porto Primavera and Itaipu Dams, Brazil. Latin American
971 Journal of Sedimentology and Basin Analysis 16, 111–118.

972 Martins, D.P., Stevaux, J.C., 2005. Formas de leito e transporte de carga de fundo do Alto Rio
973 Paraná. Revista Brasileira de Geomorfologia 6, 43–50.

974 Montanarella, L., Pennock, D.J., McKenzie, N., Badraoui, M., Chude, V., Baptista, I., Mamo, T.,
975 Yemefack, M., Aulakh, M.S., Yagi, K., Hong, S.Y., Vijarnsorn, P., Zhang, G.L., Arrouays, D.,
976 Black, H., Krasilnikov, P., Sobocká, J., Alegre, J., Henriquez, C.R., Mendonça-Santos, M. de
977 L., Taboada, M., Espinosa-Victoria, D., AlShankiti, A., AlaviPanah, S.K., Mustafa Elsheikh,
978 E.A. el, Hempel, J., Arbestain, M.C., Nachtergaele, F., Vargas, R., 2016. World's soils are
979 under threat. SOIL 2, 79–82. https://doi.org/10.5194/soil-2-79-2016

980 Mulligan, M., van Soesbergen, A., Sáenz, L., 2020. GOODD, a global dataset of more than 38,000
981 georeferenced dams. Sci Data 7. https://doi.org/10.1038/s41597-020-0362-5

982 Nagel, G.W., Novo, E.M.L. de M., Martins, V.S., Campos-Silva, J.V., Barbosa, C.C.F., Bonnet, M.P.,
983 2022. Impacts of meander migration on the Amazon riverine communities using Landsat
984 time series and cloud computing. Science of the Total Environment 806.
985 https://doi.org/10.1016/j.scitotenv.2021.150449

986 Naiman, R.J., Decamps, H., Pollock, M., 1993. The Role of Riparian Corridors in Maintaining
987 Regional Biodiversity. Ecological Applications 3, 209–212.

988 Nash, J.E., Sutcliffe, J. v, 1970. River Flow Forecasting Through Conceptual Models Part I-a
989 Discussion of Principles. J Hydrol (Amst) 10, 282–290. https://doi.org/10.1016/0022-
990 1694(70)90255-6

991 Navratil, O., Esteves, M., Legout, C., Gratiot, N., Nemery, J., Willmore, S., Grangeon, T., 2011.
992 Global uncertainty analysis of suspended sediment monitoring using turbidimeter in a
993 small mountainous river catchment. J Hydrol (Amst) 398, 246–259.
994 https://doi.org/10.1016/j.jhydrol.2010.12.025

New, M., Lister, D., Hulme, M., Makin, I., 2002. A high-resolution data set of surface climate over global land areas. Clim Res 21, 1–25.

Oestreicher, J.S., Lucotte, M., Moingt, M., Bélanger, É., Rozon, C., Davidson, R., Mertens, F., Romaña, C.A., 2017. Environmental and Anthropogenic Factors Influencing Mercury Dynamics During the Past Century in Floodplain Lakes of the Tapajós River, Brazilian Amazon. Arch Environ Contam Toxicol 72, 11–30. https://doi.org/10.1007/s00244-016-0325-1

O'Loughlin, F.E., Paiva, R.C.D., Durand, M., Alsdorf, D.E., Bates, P.D., 2016. A multi-sensor approach towards a global vegetation corrected SRTM DEM product. Remote Sens Environ 182, 49–59.

Paiva, J.B.D. de, 1988. Avaliação dos modelos matemáticos para o cálculo do transporte de sedimentos em rios. Universidade de São Paulo, São Carlos.

Paiva, J.B.D. de, Noal, A.Á., Alves, C.B., Rizzardi, A.S., Schons, C.A., Cechin, G., Libraga, J., 2011. Caracterização hidrossedimentométrica da bacia hidrográfica do rio Vacacaí Mirim, com base em dados medidos de vazão e sedimentos, in: Anais Do XX Simposio Brasileiro de Recursos Hídricos. Bento Gonçalves.

Paiva, L.E.D. de, 2007. A influência do diâmetro representativo do material de leito nas fórmulas de cálculo do transporte de sedimentos em escoamentos com superfície livre (Tese). Universidade Estadual de Campinas, Campinas.

Paiva, R.C.D., Buarque, D.C., Collischonn, W., Bonnet, M.P., Frappart, F., Calmant, S., Bulh??es Mendes, C.A., 2013. Large-scale hydrologic and hydrodynamic modeling of the Amazon River basin. Water Resour Res 49, 1226–1243. https://doi.org/10.1002/wrcr.20067

Paiva, R.C.D., Collischonn, W., Tucci, C.E.M., 2011. Large scale hydrologic and hydrodynamic modeling using limited data and a GIS based approach. J Hydrol (Amst) 406, 170–181. https://doi.org/10.1016/j.jhydrol.2011.06.007

Pelletier, J.D., 2012. A spatially distributed model for the long-term suspended sediment discharge and delivery ratio of drainage basins. J Geophys Res Earth Surf 117, 1–15. https://doi.org/10.1029/2011JF002129

Pontes, P.R.M., 2016. Modelagem hidrológica e hidrodinâmica integrada da bacia do Prata. Universidade Federal do Rio Grande do Sul.

Pontes, P.R.M., Fan, F.M., Fleischmann, A.S., Paiva, R.C.D., Buarque, D.C., Siqueira, V.A., Jardim, P.F., Sorribas, M.V., Collischonn, W., 2017. MGB-IPH model for hydrological and hydraulic simulation of large floodplain river systems coupled with open source GIS. Environmental Modelling and Software 94, 1–20.

Quinton, J.N., Govers, G., van Oost, K., Bardgett, R.D., 2010. The impact of agricultural soil erosion on biogeochemical cycling. Nat Geosci 3, 311–314. https://doi.org/10.1038/ngeo838

1032 Randle, T.J., Morris, G.L., Tullos, D.D., Weirich, F.H., Kondolf, G.M., Moriasi, D.N., Annandale,
1033 G.W., Fripp, J., Minear, J.T., Wegner, D.L., 2021. Sustaining United States reservoir storage
1034 capacity: Need for a new paradigm. J Hydrol (Amst).
1035 https://doi.org/10.1016/j.jhydrol.2021.126686

1036 Rizzardi, A.S., 2013. Avaliação e caracterização dos sedimetnos transportados no rio Vacacaí
1037 Mirim (Dissertação). Universidade Federal de Santa Maria, Santa Maria.

1038 Roulet, M., Guimarães, J.R.D., Lucotte, M., 2001. Methylmercury production and accumulation
1039 in sediments and soils of an amazonian floodplain-effect of seasonal inundation. Water Air
1040 Soil Pollut 128, 41–60.

1041 Sartori, M., Philippidis, G., Ferrari, E., Borrelli, P., Lugato, E., Montanarella, L., Panagos, P., 2019.
1042 A linkage between the biophysical and the economic: Assessing the global market impacts
1043 of soil erosion. Land use policy 86, 299–312.
1044 https://doi.org/10.1016/j.landusepol.2019.05.014

1045 Shin, S., Pokhrel, Y., Miguez-Macho, G., 2019. High-resolution modeling of reservoir release and
1046 storage dynamics at the continental scale. Water Resouces Research 55, 787–810.

1047 Shuttleworth, W.J., 1993. Evaporation, in: Maidment, D. (Ed.), Handbook of Hydrology. McGraw-
1048 Hill, New York.

1049 Siqueira, V.A., Paiva, R.C.D., Fleischmann, A.S., Fan, F.M., Ruhoff, A.L., Pontes, P.R.M., Paris, A.,
1050 Calmant, S., Collischonn, W., 2018. Toward continental hydrologic-hydrodynamic modeling
1051 in South America. Hydrol Earth Syst Sci 22, 4815–4842. https://doi.org/10.5194/hess-22-
1052 4815-2018

1053 Skofronick-Jackson, G., Petersen, W.A., Berg, W., Kidd, C., Stocker, E.F., Kirschbaum, D.B., Kakar,
1054 R., Braun, S.A., Huffman, G.J., Iguchi, T., Kirstetter, P.E., Kummerow, C., Meneghini, R., Oki,
1055 R., Olson, W.S., Takayabu, Y.N., Furukawa, K., Wilheit, T., 2017. The global precipitation
1056 measurement (GPM) mission for science and Society. Bull Am Meteorol Soc 98, 1679–
1057 1695. https://doi.org/10.1175/BAMS-D-15-00306.1

1058 Song, X.P., Hansen, M.C., Potapov, P., Adusei, B., Pickering, J., Adami, M., Lima, A., Zalles, V.,
1059 Stehman, S. v., di Bella, C.M., Conde, M.C., Copati, E.J., Fernandes, L.B., Hernandez-Serna,
1060 A., Jantz, S.M., Pickens, A.H., Turubanova, S., Tyukavina, A., 2021. Massive soybean
1061 expansion in South America since 2000 and implications for conservation. Nat Sustain 4,
1062 784–792. https://doi.org/10.1038/s41893-021-00729-z

1063 Song, X.P., Hansen, M.C., Stehman, S. v., Potapov, P. v., Tyukavina, A., Vermote, E.F.,
1064 Townshend, J.R., 2018. Global land change from 1982 to 2016. Nature 560, 639–643.
1065 https://doi.org/10.1038/s41586-018-0411-9

1066 Strasser, M.A., 2008. DUNAS FLUVIAIS NO RIO SOLIMÕES-AMAZONAS-DINÂMICA E TRANSPORTE
1067 DE SEDIMENTOS (Tese). Universidade Federal do Rio de Janeiro, Rio de Janeiro.

1068 Swanson, A.C., Bohlman, S., 2021. Cumulative Impacts of Land Cover Change and Dams on the
1069 Land–Water Interface of the Tocantins River. Front Environ Sci 9.
1070 https://doi.org/10.3389/fenvs.2021.662904

1071 Syvitski, J.P.M., Kettner, A.J., Overeem, I., Hutton, E.W.H., Hannon, M.T., Brakenridge, G.R., Day,
1072 J., Vörösmarty, C., Saito, Y., Giosan, L., Nicholls, R.J., 2009. Sinking deltas due to human
1073 activities. Nat Geosci 2, 681–686. https://doi.org/10.1038/ngeo629

1074 Syvitski, J.P.M., Vörösmarty, C.J., Kettner, A.J., Green, P., 2005. Impact of Humans on the Flux of
1075 Terrestrial Sediment to the Global Coastal Ocean. Science (1979) 308, 376–380.

1076 SZUPIANY, R., TRENTO, A., ALVAREZ, A., 2005. Transporte de Sedimentos de Fondo en el Rio
1077 Salado (Santa Fe, Argentina). Revista Brasileira de Recursos Hídricos 10, 79–88.
1078 https://doi.org/10.21168/rbrh.v10n1.p79-88

1079 Thorp, J.H., Thoms, M.C., Delong, M.D., 2006. The riverine ecosystem synthesis: Biocomplexity
1080 in river networks across space and time. River Res Appl 22, 123–147.
1081 https://doi.org/10.1002/rra.901

1082 Tilmant, A., Arjoon, D., Marques, G.F., 2014. Economic Value of Storage in Multireservoir
1083 Systems. J Water Resour Plan Manag 140, 375–383.
1084 https://doi.org/10.1061/(asce)wr.1943-5452.0000335

1085 Vörösmarty, C.J., Meybeck, M., Fekete, B., Sharma, K., Green, P., Syvitski, J.P.M., 2003.
1086 Anthropogenic sediment retention: Major global impact from registered river
1087 impoundments. Glob Planet Change 39, 169–190. https://doi.org/10.1016/S0921-
1088 8181(03)00023-7

1089 Webb, J., Mainville, N., Mergler, D., Lucotte, M., Betancourt, O., Davidson, R., Cueva, E.,
1090 Quizhpe, E., 2004. Mercury in Fish-eating Communities of the Andean Amazon, Napo River
1091 Valley, Ecuador. Ecohealth 1, SU59–SU71. https://doi.org/10.1007/s10393-004-0063-0

1092 Wei, X., Sauvage, S., Le, T.P.Q., Ouillon, S., Orange, D., Vinh, V.D., Sanchez-Perez, J.M., 2019. A
1093 modeling approach to diagnose the impacts of global changes on discharge and suspended
1094 sediment concentration within the Red River Basin. Water (Switzerland) 11.
1095 https://doi.org/10.3390/w11050958

1096 Wiegand, M.C., 2009. Proposta metodológica para estimativa da produção de sedimentos em
1097 grandes bacias hidrográficas: estudo de caso Alto Jaguaribe, CE (Dissertação). Universidade
1098 Federal do Ceará, Fortaleza.

1099 Williams, J.R., 1975. Sediment-yield prediction with Universal Equation using runoff energy
1100 factor. Present and Prospective Technology for Predicting Sediment Yield and Sources ARS-
1101 S-40, 244–252.

1102 Wisser, D., Fekete, B.M., Vörösmarty, C.J., Schumann, A.H., 2010. Reconstructing 20th century
1103 global hydrography: A contribution to the Global Terrestrial Network- Hydrology (GTN-H).
1104 Hydrol Earth Syst Sci 14, 1–24. https://doi.org/10.5194/hess-14-1-2010

1105 WU, W., 2008. Computational River Dynamics. Taylor & Francis, London.

1106 Wu, W., Wang, S.S.Y., 2006. Formulas for Sediment Porosity and Settling Velocity. Journal of
1107 Hydraulic Engineering 132, 858–862. https://doi.org/https://doi.org/10.1061/(ASCE)0733-
1108 9429(2006)132:8(858)

1109 Yamazaki, D., de Almeida, G.A.M., Bates, P.D., 2013. Improving computational efficiency in
1110 global river models by implementing the local inertial flow equation and a vector-based
1111 river network map. Water Resouces Research 49, 7221–7235.

1112 Yigzaw, W., Li, H.-Y., Demissie, Y., Hejazi, M.I., Leung, L.R., Voisin, N., Payn, R., 2018. A New
1113 Global Storage-Area-Depth Dataset for Modeling Reservoirs in Land Surface and Earth
1114 System Models. Water Resources Research TECHNICAL 54, 10,372–10,386.

1115 Yokoo, E.M., Valente, J.G., Grattan, L., Schmidt, S.L., Platt, I., Silbergeld, E.K., 2003. Low level
1116 methylmercury exposure affects neuropsychological function in adults. Environ Health 8.
1117 https://doi.org/https://doi.org/10.1186/1476-069X-2-8

1118 Zalles, V., Hansen, M.C., Potapov, P. v, Parker, D., Stehman, S. v, Pickens, A.H., Parente, L.L.,
1119 Ferreira, L.G., Song, X.-P., Hernandez-Serna, A., Kommareddy, I., 2021. Rapid expansion of
1120 human impact on natural land in South America since 1985. Sci. Adv 7. https://doi.org/DOI:
1121 10.1126/sciadv.abg1620

1122 Zarfl, C., Lumsdon, A.E., Berlekamp, J., Tydecks, L., Tockner, K., 2015. A global boom in
1123 hydropower dam construction. Aquat Sci 77, 161–170. https://doi.org/10.1007/s00027-
1124 014-0377-0

1125